Journal of Structural Geology 31 (2009) 55–71

Contents lists available at ScienceDirect

Journal of Structural Geology

journal homepage: www.elsevier.com/locate/jsg

# Primary structure influence on compositional banding in psammites: Examples from the Puncoviscana Formation, north-central Argentina

Aránzazu Piñán-Llamas [a,*], Carol Simpson [b]

[a] Department of Geological and Environmental Science, Hope College, Holland, MI 49423, USA
[b] Department of Ocean, Earth, and Atmospheric Sciences, Old Dominion University, Norfolk, VA 23529, USA

ARTICLE INFO

*Article history:*
Received 7 April 2008
Received in revised form 2 October 2008
Accepted 3 October 2008
Available online 17 October 2008

*Keywords:*
Banded psammites
Pressure-solution
Sedimentary structures
Chevron folds
Greenschist facies
Compositional banding

ABSTRACT

We investigate the influence of sedimentary structures in development of foliations in banded psammites and pelites in the meta-turbiditic Pampean Belt, Eastern Sierras Pampeanas, northwest Argentina. These anchizone to upper greenschist facies rocks were exhumed from near surface to mid-crustal levels, and preserve sedimentary structures and gradual changes in tectonic fabrics and microstructures. Primary variations in clay content affected the degree of development of a compaction-related pressure-solution cleavage ($S_P$) resulting in enhancement of the original sedimentary banding. The resulting compositional banding was overprinted by a tectonic cleavage ($S_1$) related to mid-Cambrian chevron folding. In banded sandstones, pressure-solution and mica growth that define $S_P$ and $S_1$ foliations are increasingly better developed in phyllosilicate-rich domains with increasing structural depth and metamorphic grade. Clay-rich laminae in the protolith acted as the locus for mica nucleation and growth, favoring dissolution of quartz (up to 42%) causing passive concentration of mica. Pressure-solution thus produced banded sandstones with a spaced, bedding-parallel $S_P$ cleavage in shallower sections and compositionally banded psammites and schists at depth. These observations demonstrate that formation of compositional banding does not require tectonic transposition of an older planar fabric. Similar processes may produce compositional banding in a wide range of meta-sedimentary rocks.



## 1. Introduction

Cleavage development in shaly and sandy rocks has been the subject of many studies (e.g., Means, 1975; Gray, 1978; Onasch, 1983, 1990; Engelder and Marshak, 1985; Marshak and Engelder, 1985; Gregg, 1985; Schweitzer and Simpson, 1986; Tapp and Wickham, 1987; Waldron and Sandiford, 1988; Price and Cosgrove, 1990; Wu and Groshong, 1991; Yang and Gray, 1994; Hickman and Evans, 1995; Farver and Yund, 1999; Renard et al., 2001; Fueten et al., 2002; Stallard and Shelley, 2005; Stallard et al., 2005). However, despite the numerous examples of preserved sedimentary structures in Precambrian to Paleozoic orogens, e.g., in the Dalradian rocks of Scotland (Banks and Winchester, 2004), the Helgeland Nappe Complex, of the Central Scandinavian Caledonides (Heldal, 2001), the Keseechewun Lake–Many Islands Lake area in Canada (Harper et al., 2002), and the Lachlan Orogen in Australia (Powell, 1984), only a few authors have looked at the influence of primary structures on the development of subsequent cleavage and tectonic fabrics. Maxwell (1962) and Roy (1978) postulated that diagenetic or dewatering foliations that are oblique to bedding may be associated with syn-sedimentary folding, and may even be the initial stage of slaty cleavage. Gray (1978) recognized the effect of sedimentary fabrics such as grain shape, size, orientation, and packing on cleavage type in psammites. In particular, he observed that the original grain/matrix ratio determines the type of "rough cleavage" that develops in deformed psammites. However, the full extent of the influence of primary structures on disjunctive cleavage development is still not very well understood.

Disjunctive cleavage (terminology of Powell, 1979) has been described in sandstones by several authors (see Engelder and Marshak, 1985; Murphy, 1990) also using alternative names, e.g., 'rough cleavage' (Dennis, 1972; Gray, 1978); 'deformation zones' (Boyer, 1984); and 'P-Q fabrics' (Waldron and Sandiford, 1988). Gray (1978) suggested that disjunctive cleavage (his "type C rough cleavage") develops within an initially inhomogeneous rock along primary sedimentary anisotropies such as dewatering channels or bioturbation zones. Nickelsen (1972) invoked initialization of pressure-solution on pre-existing burrows. Disjunctive cleavage has also been shown to form entirely by tectonic pressure-solution (Murphy, 1990) or by mechanical grain rotation and/or mass transfer processes acting on the crenulation of a pre-existing foliation (Borradaile et al., 1982; Worley et al., 1997; Starkey, 2002). However, aspects of spaced cleavage formation such as the

* Corresponding author. Tel.: +616 395 7227; fax: +616 395 7125.
*E-mail address:* pinanllamas@hope.edu (A. Piñán-Llamas).

0191-8141/$ – see front matter © 2008 Elsevier Ltd. All rights reserved.
doi:10.1016/j.jsg.2008.10.001

parameters that determine cleavage spacing and cleavage morphology, or the resultant rheological behavior of a polymineralic rock deforming by pressure-solution, remain enigmatic (Fueten et al., 2002). In this work, we describe how disjunctive cleavage forms at low metamorphic grade from a pre-existing sedimentary banding that is enhanced by the mechanisms of solution transfer deformation and recrystallization. We also demonstrate that development of disjunctive cleavage in sandstones is important to sandstone deformation during chevron folding.

The processes that develop compositionally layered metamorphic rocks under amphibolite and higher metamorphic conditions are also poorly understood, although such rocks make up a significant proportion of exposed continental crust, particularly in Archean cratons (Williams et al., 2000). Almost all published models involve either an ill-defined 'metamorphic segregation' (see review by Goodwin and Tikoff, 2002) or tectonic transposition of original sedimentary planar fabrics to explain the origin of compositional layers in medium- to high-grade rocks (Davidson, 1984; Jordan, 1988; Kusky and De Paor, 1988). In this paper, we demonstrate how a combination of primary bedding and diagenesis-related disjunctive cleavage produce distinctive banded psammites that, with increasing metamorphic grade, transition into compositionally banded schists. We examine Upper Proterozoic to Lower Paleozoic turbiditic rocks in the Cambrian-aged Pampean Orogen of northwestern Argentina, where there is an almost continuous transition with depth from anchizone conditions in the north to amphibolite facies metamorphism and migmatites in the south (Fig. 1). Local effects of Ordovician annealing near plutons and Andean brittle deformation are easily avoided. Thus the section is ideal for a systematic study of the influence of primary variations in mineralogy on the development of a wide range of microstructures at different structural depths in rocks of similar composition during a single tectono-metamorphic event. We argue that these processes involve significant pressure-solution differentiation, and furthermore can be used to explain similar compositionally banded psammites from a wide variety of orogenic settings.

Samples were obtained from several strike-perpendicular transects; in the absence of diagnostic mineral assemblages, deformation temperatures were estimated using natural microstructures in quartz, the experimental creep and recrystallization regimes of Hirth and Tullis (1992), and the natural deformation regimes described by Stipp et al. (2002a,b) and Rosenberg and Stünitz (2003).

## 2. Geological setting

The Upper Proterozoic to Lower Paleozoic Puncoviscana Formation (Durand and Aceñolaza, 1990; Rapela et al., 1998a) forms a major component of the north central Argentine Pampean Orogen (Fig. 1; Pankhurst et al., 1997; Rapela et al., 1998b; Keppie and Bahlburg, 1999). These turbiditic rocks were initially deposited in a thick accretionary prism on the margin of Gondwana after the break-up of Rodinia and were off-scraped and accreted to the Gondwana margin during the Cambrian-aged Pampean orogenic event (Piñán-Llamas and Simpson, 2006). The Puncoviscana Fm. *sensu stricto* is a relatively unmetamorphosed turbiditic sequence that crops out near the Bolivian border (22–26°S; 65–67°W; Turner, 1960) and has been shown to extend into equivalent and gradually higher-grade rocks to the south (Piñán-Llamas and Simpson, 2006). Neither total thickness, nor basement to the sequence, is known. Analyses of idiomorphic detrital zircons from volcaniclastic beds in the middle of the non-metamorphic section, in the northern part of the orogen, indicate a depositional age range of 530–560 Ma (Lork et al., 1990), although in southern (structurally deeper) sections the depositional age may be older (~600 Ma, Sims et al., 1998; Rapela et al., 1998b; Schwartz and Gromet, 2004). The depositional age of the Puncoviscana Fm. *s.s.* is also constrained by the presence of Tommotian-Vendian (Upper Proterozoic/Lower Cambrian) ichnofauna – *Helminthopsis*, *Planolites*, *Oldhamia*, *Diplichnites*, *Squamodictyon*, and *Tiernavia* – that confirm a deep-sea environment (Aceñolaza, 1978; Aceñolaza and Durand, 1986; Durand and Aceñolaza, 1990; Omarini et al., 1999; Aceñolaza, 2004; Aceñolaza and Aceñolaza, 2007).

Pervasive chevron folding of the entire Puncoviscana Fm. during the Pampean Orogeny was accompanied by formation of a fold-related cleavage ($S_1$) that is better developed with structural depth (Piñán-Llamas and Simpson, 2006), and which overprints an earlier, diagenesis-related disjunctive cleavage that is the subject of this paper. Published K/Ar whole rock metamorphic ages obtained from Puncoviscana Fm. pelites range from 550 to 535 Ma in locations north of Tucuman (Fig. 1), to $565 \pm 7$ Ma near Tucuman (Adams et al., 1990). Folding was followed by intrusion of scarce I-type granites, such as the $526 \pm 2$ Ma (U–Pb age, Hongn et al., 2001) Santa Rosa de Tastil pluton (Fig. 1), and by uplift and erosion prior to deposition of the unconformably overlying Middle Cambrian Meson Group (Turner and Mon, 1979; Rossi de Toselli et al., 1992; Hongn et al., 2001).

Subsequent development of a magmatic arc to the west of the Pampean orogen occurred during the Ordovician (Famatinian orogeny; Pankhurst et al., 1998; Saavedra et al., 1998) and younger, arc-related microplates accreted during the Devonian (Achalan Orogeny; Whitmeyer and Simpson, 2004). However, within the Pampean orogen, the effects of both the Ordovician and Devonian events are localized and mainly involve large-scale, but discrete shear zones (Whitmeyer and Simpson, 2003) and post-tectonic plutons that intruded the folded rocks and produced contact aureoles tens of meters to 2 km wide with local static annealing and overgrowth of unoriented andalusite, garnet, and staurolite porphyroblasts. Thus, large areas of the Pampean orogen were essentially unaffected by these younger events. Separation of the orogen into isolated fault blocks with intervening sediment-filled, pull-apart basins began in the late Carboniferous and continued through the Cretaceous (Simpson et al., 2001), culminating with uplift and tilting during the Tertiary to Recent Andean Orogeny (Jordan and Allmendinger, 1986).

Present-day exposures of the Puncoviscana Formation *s.s.* and related rocks (Fig. 1) exhibit an almost continuous transition from anchimetamorphic shales and greywackes in the northern part of the orogen, to upper greenschist facies pelites and psammites in the central region (Ancasti, Fig. 1), in which bedding and sedimentary structures are still identifiable, to amphibolite facies schists in southern exposures, in which all identifiable sedimentary structures have been obliterated. The metamorphic transition has been attributed to increasing original depth in the orogen coupled with local proximity to thermal domes (Willner and Miller, 1985; Willner, 1990; Piñán-Llamas and Simpson, 2006). Several authors have discussed the metamorphic reactions in the metaturbidites (e.g., Toselli and Weber, 1982; Toselli and Rossi de Toselli, 1984; Do Campo and Omarini, 1990; Do Campo et al., 1994). Willner and Miller (1982) were the first to consider tectonic transposition as responsible for the origin of a ubiquitous and distinctive compositional banding in psammites in Sierra de Ancasti (Fig. 1). However, in the following sections we show that this compositional banding is a consequence of the superposition of a bedding-parallel, pre-tectonic solution cleavage onto primary bedding. We initially document the primary and pre-tectonic structures, which are best exposed in the northern part of the orogen, before describing how these structures have influenced the subsequent tectonic cleavage. In our work we interpret increasing metamorphic grade, as defined by stable mineral assemblages, metamorphic equilibrium textures,

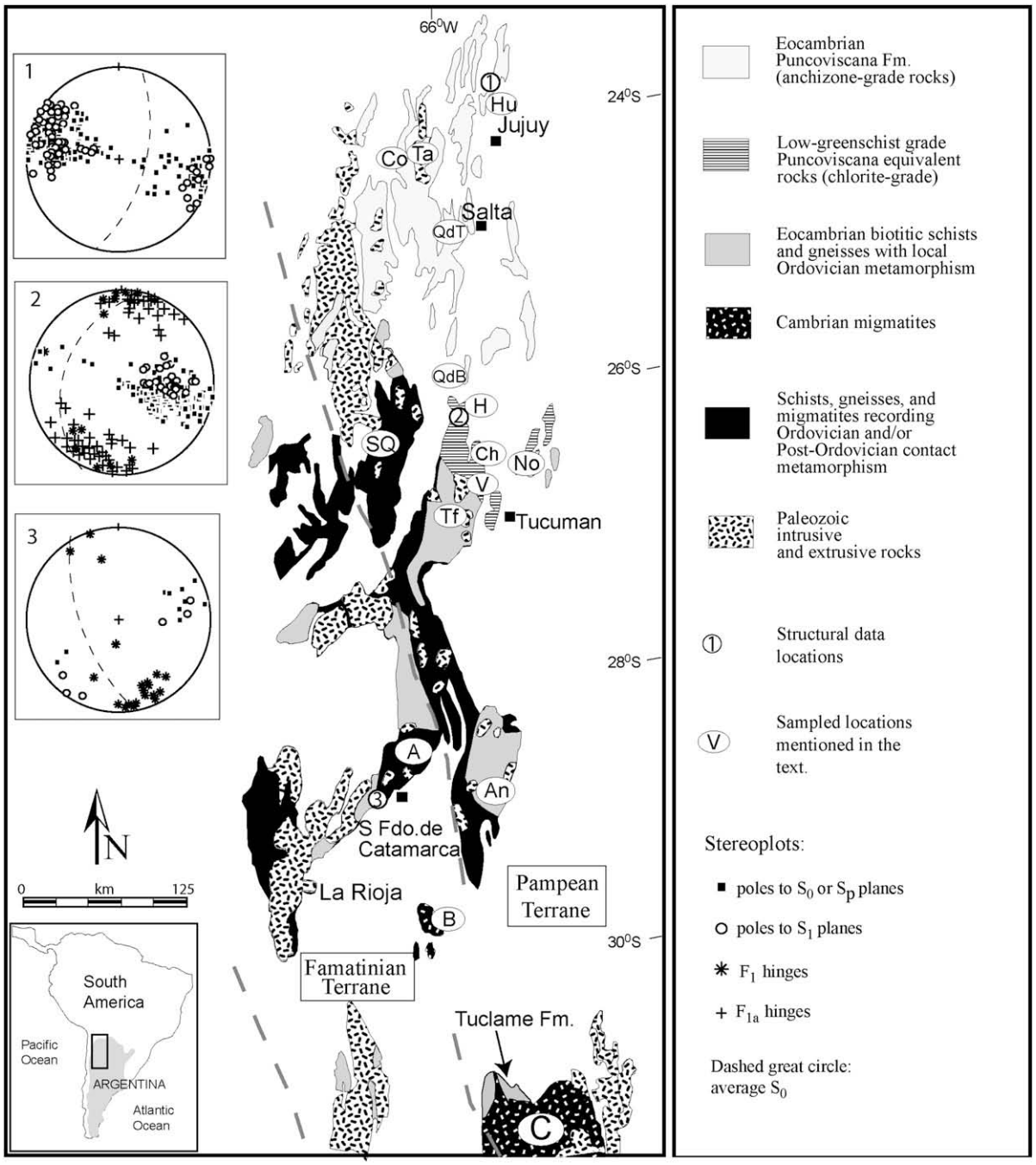


**Fig. 1.** Simplified geological map of Lower Paleozoic rocks in NW Argentina (see inset) modified from Willner and Miller (1985), Becchio and Lucassen (2002), and Simpson et al. (2003). Dashed lines indicate approximate boundaries between peri-Gondwanan terranes. The Pampean Terrane includes the Puncoviscana Formation and its higher-grade metamorphic equivalents to the south. Representative structural data plotted on lower hemisphere equal angle stereographic projections: (1) Tilcara, $S_0$ $n = 149$, $S_1$ $n = 67$; (2) Hualinchay, $S_0$ $n = 163$, $S_1$ $n = 24$, $F_1$ hinges $n = 15$; (3) San Fernando de Catamarca, $S_0$ $n = 10$, $S_1$ $n = 6$, $F_1$ hinges $n = 21$. Localities: A, Ambato; An, Ancasti; B, Brava; C, Córdoba; Ch, Choromoro; Co, San Antonio de los Cobres; H, Hualinchay; Hu, Humahuaca; No, Nogalito; QdB, Quebrada de Don Bartolo; QdT, Quebrada del Toro; S, Siambon; SQ, Sierra de Quilmes; Ta, Santa Rosa de Tastil; Tf, Tafí del Valle; V, Vipos.

and preserved quartz microstructures, with structural depth in the section. To ensure appropriate petrographic comparisons, we avoided using samples from the aureoles of exposed igneous intrusions.

## 3. Primary structures

The sedimentology of the Puncoviscana Formation *s.s.* has been previously discussed in detail by Omarini (1983), Omarini and Baldis (1984), Jezek (1986, 1990), and Omarini et al. (1999) among others. These deposits, that predominantly consist of Tbc and Tbcde Bouma sequences (Jezek and Miller, 1987), were likely derived from cratonic parts of southwest Gondwana (Aceñolaza et al., 1988; Schwartz and Gromet, 2004), and reflect distal, shallowing-upward, progradational sequences interrupted by episodic influxes of storm sand (Omarini et al., 1999). Bed contacts are usually either erosive or transitional, and layers are laterally continuous and lack channel deposits. The proportions of shale to sandstone vary with locality. The surface of each storm bed was bioturbated by a variety of organisms (Jezek and Miller, 1987).

Published X-ray diffraction data from Humahuaca, San Antonio de los Cobres (Fig. 1; Toselli and Weber, 1982), and Quebrada del Toro samples (Fig. 1; Do Campo and Omarini, 1990; Do Campo et al., 1994, 1998; Do Campo and Nieto, 2003) indicate that mineral associations present in the Puncoviscana Formation *s.s.* are Ill + Ms + Chl + Qtz + Pl(Ab) (abbreviations for mineral names from Kretz, 1983). Due to the small grain size of phyllosilicates, illite crystallinity is the only reliable indication that the metamorphic grade in these rocks reached mid- to uppermost anchizone conditions, with temperatures of at least 270 °C (Toselli and Rossi de Toselli, 1982; Toselli, 1990; Do Campo, 1999).

In the turbiditic deposits, thin bedded (3–30 cm) fine-grained sandstones show a wide variety of sedimentary structures: graded bedding, cross lamination (Fig. 2a) and parallel lamination, lenticular beds, flame structures, load casts (Fig. 2b), and flaser bedding. In contrast, meter-thick, medium to large grained, massive sandstones that have been classified as greywackes and lithic greywackes (Jezek et al., 1985) are generally poorly graded and have scarce sedimentary structures.

In thin section, massively bedded greywackes, e.g., from Quebrada del Toro (QdT in Fig. 1; photomicrograph, Fig. 3a; sample 56 in Appendices A and B), exhibit clasts of up to 1 mm in diameter that are angular, inequant, and unoriented, occasionally with incipient mica beards. In outcrops to the south, e.g. Quebrada de Don Bartolo (QdB in Fig. 1; photomicrograph, Fig. 3b; Sample Punco1 in Appendices A and B), greywackes contain well-developed mica beards and locally, a well-defined grain alignment that defines a foliation ($S_p$) parallel to $S_0$. $S_p$ is also defined by discontinuous chlorite and white mica seams aligned parallel to bedding that wrap around (and are best defined at the margins of) 50–400 μm subrounded clasts. Clasts have sinuous, interpenetrated boundaries. Few elongate quartz and feldspar clasts are preferentially aligned with $S_0$.

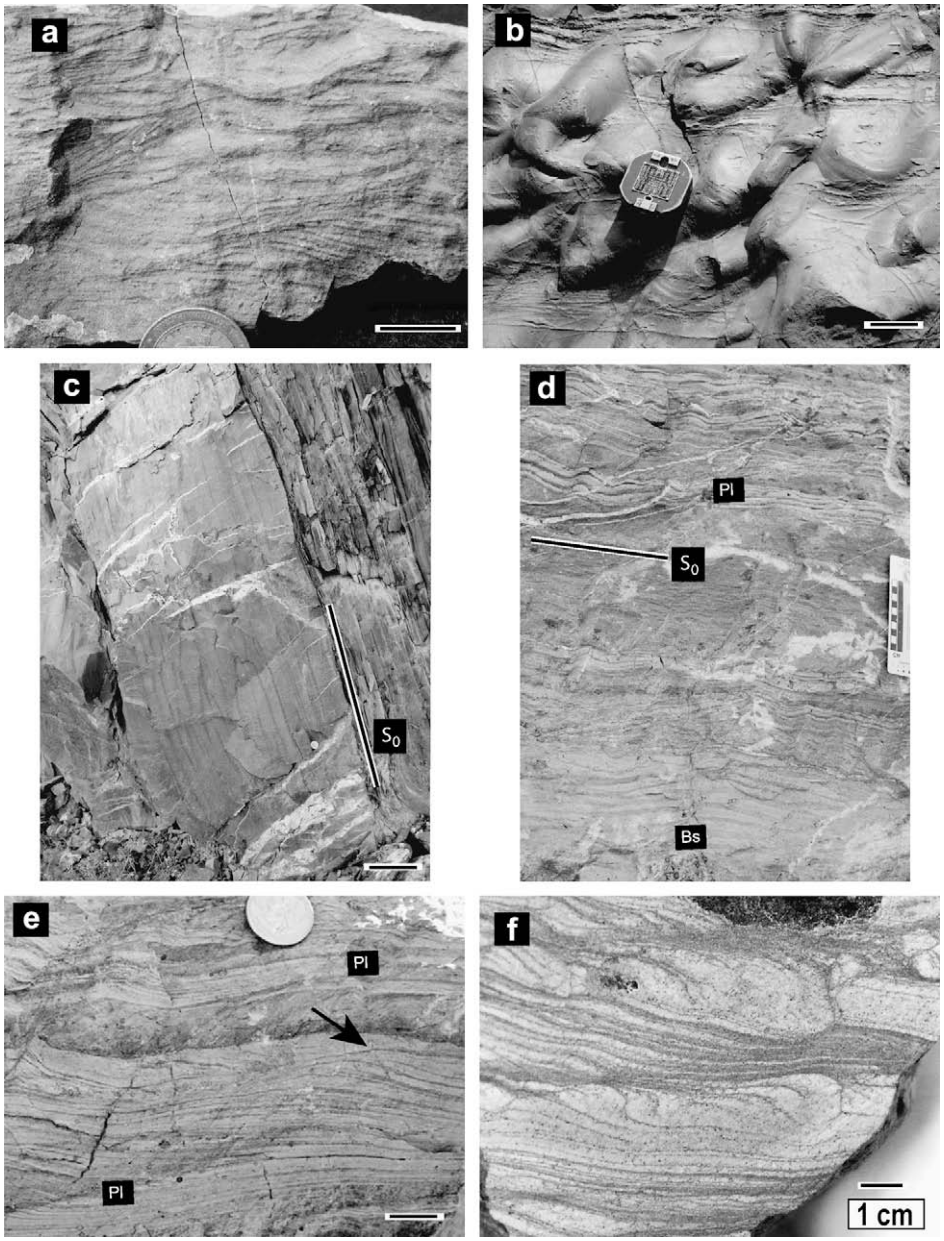


**Fig. 2.** Outcrop photos of sedimentary structures in turbiditic Puncoviscana Formation and chlorite-grade equivalents. Locations on Fig. 1. (a) Cross-bedding in fine-grained sandstone, Quebrada del Toro. (b) Load casts on sandstone bed base, Humahuaca. (c) Tabular beds of anchizone-grade parallel banded sandstones, Humahuaca. (d) Bedding ($S_0$) in chlorite-grade banded psammites (Bs) grade into fine-grained metasandstones and shales with parallel lamination (Pl), Hualinchay. (e) Detail of parallel- (Pl) and cross-laminations (arrowed) from same outcrop as (d). (f) Slump folds preserved in fine-grained chlorite-grade metasandstone, Hualinchay. Scale bars (a,e) 2 cm, (b) 5 cm, (c) 10 cm.

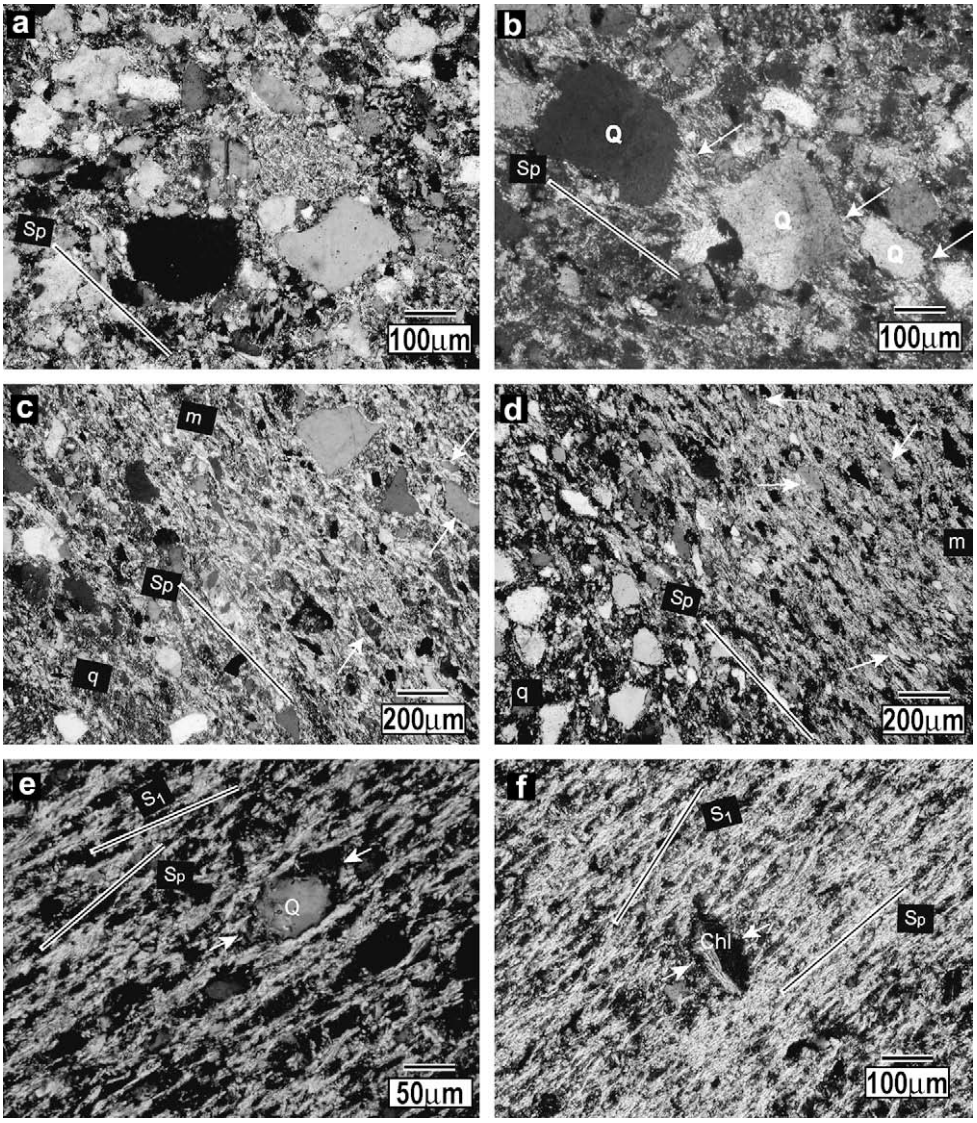


**Fig. 3.** Photomicrographs (nicols crossed) of banded and massive sandstones with incipient $S_p$ (a–c), and pelites and psammites with well-developed $S_p$ (d–f). Localities on Fig. 1. (a) Massive anchizone sandstone (Quebrada del Toro). Weak $S_p$ defined by white mica. (b) Massive anchizone sandstone (Quebrada de Don Bartolo). Weak $S_p$ defined by white mica and by mica 'beards' (arrowed) on quartz (Q) clasts. (c) Banded anchizone-grade sandstone (sample 67A from Humahuaca). Macroscopic banding ($S_p$) defined by oriented clays, detrital micas, and chlorite in mica-rich domains (m) and by interspersed clays and detrital micas in quartz-rich domains (q). Some elongate subangular quartz and detrital feldspar (arrowed) in m-domains are aligned parallel to $S_p$. (d) Banded chlorite-grade psammites (sample 84B from Hualinchay). Mica-rich domains (m) with strong $S_p$ contain high aspect ratio quartz grains with dissolved margins (arrowed); quartz-rich domains (q) contain angular, equant quartz grains. (e) Chlorite-grade pelite with well-developed $S_p$ defined by white mica and chlorite (Hualinchay). Quartz grain (Q) shows pressure shadows (arrowed). (f) Chlorite-grade pelite (Choromoro) with $S_p$ defined by white mica and chlorite. Large chlorite grain (Chl) has basal planes at high angle to $S_p$ and asymmetrical pressure shadows (arrowed). Incipient $S_1$ in (e) and (f) defined by re-oriented white micas.

Within the turbiditic sequence, banded sandstones (Fig. 2c) grade into parallel- and cross-laminated siltstones and sandstones, and thinly laminated siltstones with centimeter-scale structures interpreted as slumps. Banded sandstones consist of 2–5-mm thick clay-rich domains alternating with 13-cm thick quartz-rich domains. Clay-rich and quartz-rich bands are parallel or subparallel to bedding.

In thin section, clay-rich domains include phyllosilicates (clays and small white mica grains) that are aligned subparallel to bedding (Fig. 3c) and wrap around 15–50 μm sized inequant and subangular to angular quartz and feldspar clasts and rock fragments. Within the clay-rich bands, only a few quartz and feldspar grains are elongate and aligned subparallel to bedding (Fig. 3c). Quartz-rich bands have a composition similar to a greywacke (see Appendix A), with quartz and feldspar grains and rock fragments that are poorly sorted, more angular, larger, with fewer interpenetrated borders, and more randomly oriented (Fig. 3c) than clasts in clay-rich bands. The contact between quartz-rich domains and clay-rich domains in banded sandstones is gradational and everywhere parallel to bedding. Locally, quartz-rich bands are graded and capped with clay-rich laminae. Thus, the compositional banding in sandstones is inferred to be primary.

## 4. Pre-tectonic enhancement of compositional banding

### 4.1. Chlorite grade

An increase in metamorphic grade within more southerly outcrops of the Puncoviscana Formation (i.e. Hualinchay, Choromoro; Fig. 1) is indicated by the mineral associations Chl + Ms + Qtz + Pl(Ab) in pelites and Qtz + Kfs + Pl(Ab) + Ms in psammites/greywackes. Based on illite crystallinity values and the presence of iron-rich chlorite in rocks near Tucuman (Fig. 1), Toselli and Rossi de Toselli (1983) suggest that rocks in this area reached

275–350 °C (chlorite grade). Mineral changes from anchizone to chlorite grade are accompanied by a general increase in mica grain size, in both mica-rich and quartz-rich domains, and an increasing abundance of muscovite. The new metamorphic minerals are aligned subparallel to bedding consistent with burial to deeper crustal levels.

In sections of the Puncoviscana Formation that have reached greenschist facies, it is possible to observe banded psammites grading into laminated siltstones (Fig. 2d). Fine-grained psammites preserve lenticular, parallel, and trough cross-bedding (Fig. 2e), slump folds (Fig. 2f), and flame and flaser structures. In thin section, cross-beds are seen to be defined by graded quartz-rich laminae that alternate with thin, chlorite- and white mica-rich laminae and thin layers of opaque minerals and zircons.

In banded psammites, quartz-rich bands of variable thickness (0.4–2 cm) that have a composition similar to greywacke (see Appendix A) alternate with mica-rich domains (0.1–4 mm) that are parallel or subparallel to bedding. Within mica-rich domains, micas anastomose around elongate quartz grains that show evidence of pressure-solution along grain edges parallel to $S_0$ (Fig. 3d). Clasts within mica-rich domains exhibit higher axial ratios (2:1 to 8:1; Fig. 3d), more sinuous borders, and stronger grain shape preferred orientation than clasts in the quartz-rich bands (Fig. 3d). Within the poorly sorted to graded quartz-rich domains, quartz, feldspar, and rock fragment clasts are larger (15–50 μm in diameter), more inequant, and more angular than clasts in the mica-rich bands. Compared to anchizone rocks, mica beards on detrital clasts, large interspersed metamorphic chlorites and white micas (50–200 μm long), and pressure-solution residue seams become more abundant within the quartz-rich bands and define a foliation, $S_p$, parallel to bedding ($S_0$). Also with increasing temperature, pelitic lithic fragments become more scarce (Appendix A), and portions of the matrix are recrystallized into new quartz grains with metamorphic chlorite and muscovite. Quartz and feldspar clasts develop interpenetrated borders and quartz overgrowths parallel to $S_0$ are common.

In pelites, a well-developed, continuous cleavage ($S_p$), parallel or subparallel to $S_0$, is defined by aligned detrital micas and chlorite flakes that range in length from 15 to 150 μm. Interspersed elongate, symmetrical, and isolated quartz, feldspar, and lithic clasts have smooth interfaces with mica grain boundaries parallel to $S_0$ (and $S_p$). These isolated grains also exhibit chlorite fibers in 'pressure shadows' parallel to $S_0$ (Fig. 3e). Quartz clasts show no apparent lattice-preferred orientation when a gypsum plate is used with cross-polarized light. Locally, large chlorite grains and chlorite–mica stacks (50–75 μm long) have basal planes sub-perpendicular to $S_0$ and $S_p$, and also show pressure shadows of extremely fine-grained chlorite and/or quartz (Fig. 3f).

In locations near Tucuman (e.g., in Vipos, Fig. 1), $S_p$ in massively bedded psammites is defined by abundant, aligned, 25150 μm grains of muscovite and chlorite, by pressure-solution seams, and by symmetrical, elongate quartz grains that have dissolved borders where they are in contact with phyllosilicate grains. Lattice preferred orientation is not apparent among quartz clasts or matrix grains when using a gypsum plate.

### 4.2. Biotite grade

In the highest grade samples (Nogalito, Tafi del Valle, Fig. 1) the assemblage Qtz + Kfs + Bt + Ms + Pl(Ab) occurs, for which we suggest the reaction Chl + Kfs = Bt(Ann) + Ms + Qtz + $H_2O$. In the KFASH system ($K_2O$–FeO–$Al_2O_3$–$SiO_2$–$H_2O$), this reaction takes place at low- to mid-greenschist facies conditions (~400–425 °C at about 3.5 kbar; Mather, 1970; Miyashiro and Shido, 1985).

Unambiguous small-scale sedimentary structures have not been found in the biotite- or higher-grade sections. Nevertheless, original macro-scale bedding (Fig. 4a) is preserved in sequences that include 5-cm to 2-m thick layers of banded biotite schists and 0.4-m to several meters thick meta-greywacke layers. In these sequences, the banded biotite schists exhibit a pervasive, monotonous, and highly distinctive compositional banding subparallel to bedding, defined by centimeter thick lenticular quartz-rich bands that alternate with 2–5-mm thick biotite-rich layers, e.g. in the Ancasti range (Figs. 1, 4b) or in the Nogalito range (Figs. 1, 4c; Appendices A and B). These lenticular bands are extremely similar in appearance to sedimentary bands and bedding laminae in lower-grade sections (Fig. 2d,e), where primary structures are well preserved.

In thin section, quartz-rich bands in banded biotite schists exhibit subequant to elongate quartz grains that show no lattice preferred orientation with the gypsum plate, with interspersed tabular biotites (30–200 μm) oriented parallel to band margins (Fig. 4d). The matrix has been recrystallized, and pelitic rock fragments have not been observed (see Appendices A and B). However, detrital quartz and feldspar clasts with undulatory extinction and pressure-solution seams parallel to the compositional banding are preserved. Biotite-rich bands are usually thinner than adjacent quartz-rich bands, are oriented parallel to the original macro-scale bedding, and include corroded and typically internally deformed biotite grains, 50 μm to 1 mm long, with quartz and feldspar grain inclusions. As we discuss later, we infer that this compositional banding is equivalent to the disjunctive $S_p$ foliations seen in the lower-grade psammites of the region.

## 5. Chevron fold-related cleavage

Ubiquitous, meter- to decameter-scale, upright horizontal chevron folds ($F_1$) with generally NNE–SSW trending hinges (Fig. 1), affect the turbiditic rocks along the entire length of the orogen. Chevron folds ($F_1$) formed at an early stage during the middle Cambrian (Pampean) Orogeny (Simpson et al., 2001; Piñán-Llamas and Simpson, 2006). In deeper and more southerly sections of the orogen (e.g., Tafi, Ancasti; Fig. 1) parasitic $F_1$ folds are present. The orientation of $F_1$ hinges in these more southerly sections is NNW/SSE, and most likely reflects the rotation of the blocks during post-Pampean tectonic events. Associated with $F_1$ is a tectonic cleavage ($S_1$) that increases in degree of development with increasing temperature and depth in the orogen.

### 5.1. $S_1$ in anchizone grade locations

In the northern, anchizone sections (e.g., Tilcara, Fig. 1), upright chevron folds have straight limbs (Fig. 5a) and no parasitic folds. The only centimeter-scale asymmetrical folds observed are slumps of finely laminated sandstone and siltstone that are restricted to local sedimentary horizons and bounded by overlying and underlying flat siltstone beds; slump fold axes are not parallel to $F_1$ axes, and $S_1$, where present, cross-cuts them at angles from 15° to 45°.

Chevron folds exhibit a simple disjunctive cleavage ($S_1$) that is first observed in siltstones only, at approximately 1–2 cm spacing (Fig. 5b). In thin section, $S_1$ is defined in the siltstones by aligned chlorite and new white mica grains (25–100 μm) that become progressively larger to the south (e.g., Quebrada de Don Bartolo, Fig.1) as $S_1$ gradually changes into a well-developed, fanning, continuous cleavage. $S_1$ is oblique to $S_0$ (and therefore to $S_p$) at angles ranging from 10–15° to 30–45° on chevron fold limbs. Occasional large chlorite grains and chlorite–mica stacks with basal planes subperpendicular to bedding are kinked, sheared, or tilted at different angles with respect to $S_p$ (tilt angles range from 0° to 90°, although the range 90° to 45° is predominant), and also have pressure shadows that contain extremely fine-grained chlorite and/or quartz.

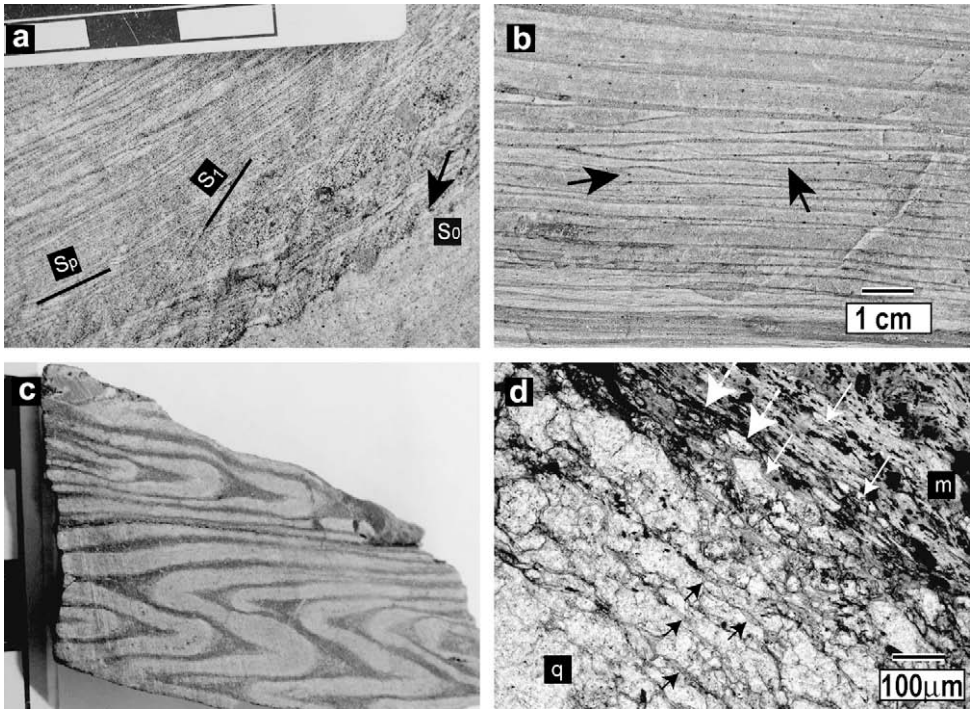


**Fig. 4.** Biotite grade banding in psammites and schists. Localities in Fig. 1. (a) Banded biotite schist (Tafí del Valle). Compositional bands parallel and subparallel to relict bedding (arrowed). (b) Lenticular banding (arrowed) in biotite schist (Ancasti). (c) Folded lenticular layers resembling slump structures in biotite schist (Nogalito). (d) Photomicrograph (plane light) of banded biotite schist (sample NOG from Nogalito) with quartz-rich (q) and mica-rich (m) domains. In quartz-rich bands, interspersed tabular biotites (small black arrows) are oriented parallel to the band margins. Mica-rich bands include elongate grains (large arrows) and solution seams (dashed arrows).

In compositionally banded psammites, the fold-related $S_1$ cleavage is weakly defined and preferentially localized in mica-rich domains where $S_1$ intersects $S_0$ (and $S_p$) at 15–20°. Within quartz-rich domains, $S_1$ is weakly defined by individual new muscovite and chlorite grains (100–200 μm) that are oriented at 35–40° with respect to $S_p$.

### 5.2. $S_1$ in chlorite grade locations

In chlorite-grade compositionally banded psammites, $S_1$ is defined in both mica-rich and quartz-rich domains by metamorphic micas and chlorite grains aligned at 35–40° with respect to $S_p$ (Fig. 5c), by asymmetric quartz and feldspar clasts with pressure shadows, and by thin layers of oxide deposits (pressure-solution seams). The more massive psammites exhibit an irregularly spaced (~1–2 cm), fanning (e.g., Hualinchay, Fig. 1), discrete $S_1$ cleavage that is also progressively more pervasive, more continuous, and better defined to the south (e.g., Vipos, Fig. 1).

### 5.3. $S_1$ in biotite grade locations

In biotite-grade psammites, $S_1$ is locally evident as a disjunctive crenulation cleavage formed by microfolding of mica-rich $S_p$ domains and recrystallization of new metamorphic biotites on the microfold limbs (Fig. 5d). In Tafi del Valle (Fig. 1), centimeter-scale parasitic $F_1$ folds exhibit an $S_1$ axial planar cleavage that consists of euhedral tabular biotite grains aligned in thin cleavage bands that cross-cut and therefore post-date the compositional banding.

In biotite-grade banded schists from the Nogalito area (Fig. 1), $S_p$ is defined by biotite-rich bands that contain quartz grains and rock fragments with high axial ratios and pressure-solution seams (Fig. 6a). In quartz-rich bands, $S_p$ is defined by pressure-solution seams (Fig. 6b) and by small micas and elongate quartz grains oriented parallel to compositional banding. Centimeter-scale $F_1$ parasitic folds that fold $S_p$ (Fig. 4c) exhibit an $S_1$ cleavage that is sygmoidal to slightly oblique to $S_p$ and locally overprints $S_p$ in quartz-rich bands on fold limbs (Fig. 6c). In this location, $S_1$ is defined by oriented biotite and muscovite grains (150–200 μm long), by opaque-rich pressure-solution seams, and by incipient dynamically recrystallized, elongate quartz grains with long dimensions oblique to fold limbs and to $S_p$. Sutured grain boundaries (Fig. 6d) are consistent with Regime I recrystallization (Hirth and Tullis, 1992) operating locally in addition to pressure-solution. In contrast, subequant and subrounded detrital quartz and feldspar grains are present in the fold hinges (Fig. 6c) where $S_1$ pressure-solution seams are very weakly expressed. Insertion of a gypsum plate in the microscope under crossed polarized light indicates that there is no lattice preferred orientation of quartz or feldspar grains in either fold limbs or hinges.

## 6. Strain estimates

Seven banded psammites were chosen for detailed strain and volume loss analysis from the limbs of upright chevron folds in order to determine the strain accumulated during $S_p$ and $S_1$ cleavage formation under different metamorphic conditions (Fig. 7; see Appendices A and B). Sample 67A is a banded sandstone metamorphosed under anchizone conditions; it exhibits no apparent lineation. Samples 54, 84B, and 76A are greenschist facies banded psammites that show an increasing amount of white metamorphic mica and development of $S_1$ cleavage with increase in metamorphic grade. Although sample 76A is located in the chlorite-grade region on Fig. 7a, it contains a few biotite grains. Two additional greenschist facies samples, 94A and 77, exhibit a weak mineral lineation. NOG is a banded biotite schist (Figs. 4c, 7; Appendices A and B).

Thin sections were cut perpendicular to bedding and thus to the compositional banding, and normal to fold hinges (or parallel to the mineral lineation, where present). In samples 94A and 77, two mutually perpendicular sections, 94A-2 and 77B were cut normal to bedding and parallel to fold hinges.

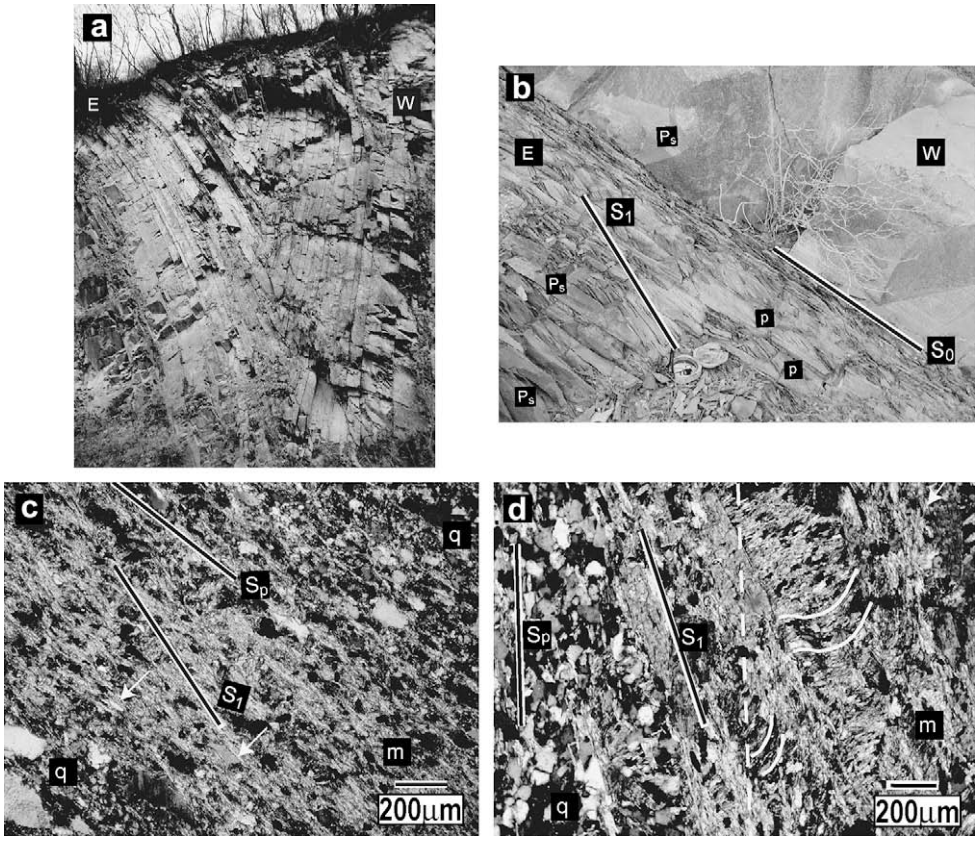


**Fig. 5.** Development of $S_1$ and its relationship to post-$S_p$ chevron folds. Localities in Fig. 1. (a) Chevron fold in tabular chlorite-grade arenites, shales and greywackes (Choromoro). W, west; E, east. (b) Anchizone grade psammites (Ps) and pelites (p) with $S_1$ development in the latter at moderate angle to $S_0$. (c) Photomicrograph of $S_1$ in chlorite-grade banded psammites (sample 76A from Hualinchay). Mica-rich domains (m) contain quartz grains with dissolved margins (arrowed) and high axial ratios cf. grains within quartz-rich (q) domains. $S_p$ is defined by the elongate grains and by the preferred orientation of micas in the mica-rich bands. $S_1$ is defined by aligned white micas, and transects both m and q bands post-dating the compositional banding. (d) Photomicrograph of $S_1$ in biotite-grade banded schist (Ancasti). $S_p$ defined by alternating quartz-rich (q) and mica-rich bands (m). For clarity, the mica-rich/quartz-rich boundary has been highlighted with a white dashed line. White continuous lines highlight mica basal planes within $S_p$ that have been microfolded. Aligned biotites oblique to the mica-rich band developed on crenulation limbs defining a localized $S_1$ that postdates the compositional banding. Nicols crossed in (c,d).

### 6.1. Dissolved quartz

Chlorite-grade and biotite-grade banded psammites show microstructural changes, including shape change in quartz grains within mica-rich domains, that reflect enhancement of the bedding-parallel $S_p$ observed in anchizone regions. To estimate the amount of shortening accommodated by dissolution of quartz grains in banded psammites, we made comparative volume loss measurements from four banded psammites (Table 1; Fig. 7; see Appendix A) where the mica-rich and quartz-rich bands occur with similar proportions. Whole-rock chemical analyses of three of the banded psammites are also included in Appendix C.

Within each thin section, detrital quartz grains with long axes sub-parallel to bedding were analyzed in (i) a representative mica-rich band, and (ii) an adjacent quartz-rich band. Fifty grains were analyzed within each band; a total of 100 grains were analyzed for each thin section. The area of an ellipse circumscribing each grain was measured as an estimate of original undissolved area. We consider this measurement conservative as a predominance of relatively equant quartz grains in the mica-poor domains of anchizone samples suggests that original grains might have originally been more circular in cross-section. The areas of the grains and the smooth circumscribing ellipses were calculated using the NIH's ImageJ computer program. To check for extension perpendicular to the stretching axis in these samples, we also performed Fry analysis on two perpendicular thin sections from each sample (Section 6.2); the results show that there is no significant difference in shortening values in both directions (Table 2). The absence of fabric elements such as fibers and grain overgrowths in thin sections normal to bedding and parallel to fold hinges also suggest that there has been no extension in the plane normal to shortening direction. Thus, in the analyzed samples, we infer no extension perpendicular to the axis of shortening ($X = 1$; $Y = 1$; $Z < 1$) and, therefore, that the ratio of grain area to ellipse area yielded a minimum estimate of the percentage volume lost from dissolution of quartz grains in three dimensions.

In all samples, mean values of dissolved quartz grains are always higher in the mica-rich bands and these mean values increase with depth. Also with increasing depth, the standard deviation within mica-rich bands increases (Table 1), but the standard deviation decreases for quartz-rich bands, perhaps indicating a more homogeneous strain than in the mica-rich bands.

Comparative measurements show that quartz grains in mica-rich bands underwent approximately 26% volume loss in low-grade samples and 42% volume loss in higher-grade samples, whereas in quartz-rich bands, volume losses were about 16% in low-grade and 29% in higher-grade samples. Because we assume a circumscribing ellipse as the original cross-sectional grain shape, rather than a circumscribing circle, these are minimum estimates of dissolution. Nevertheless, we can conclude that dissolution of quartz grains is more important in mica-rich bands (Fig. 7b) and generally increases with metamorphic grade, which we equate to depth in the section.

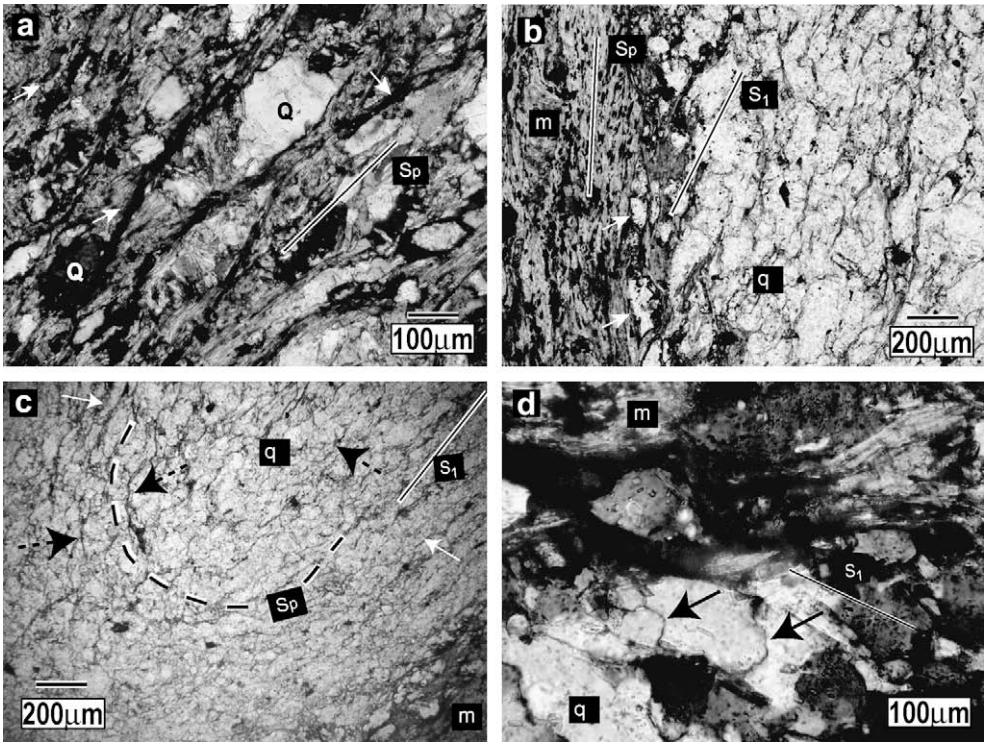


**Fig. 6.** Superposition of $S_1$ onto $S_p$ in $F_1$-folded schist (sample NOG from Nogalito, Fig. 1). (a) Enlargement of a mica-rich band ($S_p$) with high aspect ratio of quartz grains (Q) and seams of insoluble residues (arrowed). (b) $S_p$ defined by mica-rich domains (m) with oxide seams and elongate, but unstrained, interspersed quartz grains (arrowed). Grain shape preferred orientation in quartz-rich bands (q) defines $S_1$ which is oblique to compositional banding. (c) Equant quartz and feldspar grains in fold hinge zone (dashed line). Quartz grains on fold limbs are locally very elongate (arrowed). Pressure-solution seams (dashed arrows) in quartz-rich bands (q) are subparallel to the mica-rich bands (m), which are folded by $F_1$. (d) Enlargement of a mica-rich (m) quartz-rich (q) boundary in the Nogalito biotite schists. Quartz grains show lobate borders (arrowed) typical of grain boundary migration. Nicols crossed in (c,d), plane light in (b,c).

### 6.2. Fry analysis

Seven banded psammites (67A, 54, 84B, 94A, 77, 76, NOG) were chosen for Fry analysis. Using a Nikon Coolpix digital camera, six digital photomicrographs were taken from most of the thin sections (in the banded psammites only quartz-rich bands were photographed) to ensure representative areas for analysis. In sample 76A, just 4 photomicrographs were taken due to the paucity of particles suitable for Fry analysis. To maximize contrast on the computer screen, cross-polarized light was enhanced by inserting a +530 nm gypsum plate. Brittle deformation can modify the original grain shape and therefore invalidate strain measurements, therefore areas with brittle microstructures were avoided as were primary structures, as particles with a preferred orientation prior to deformation can obscure tectonic fabrics (Ramsay and Huber, 1983). The sandstones and banded psammites were analyzed using Fabric7 (http://www.geolsoft.com) and De Paor (1989, 2001) Fry Analysis programs. At least 60 grains were digitized on each photomicrograph to produce valid Fry plots.

The original method of Fry analysis (Fry, 1979; Hanna and Fry, 1979) was designed to work with large populations (100–200) of objects that were initially isotropic and strongly anti-clustered. Crespi (1986) determined that about 50 points should lie in an annulus covering 10% of the radius of the central vacancy in order for that vacancy to be well defined (see also Meere and Mulchrone, 2003).

Other concerns with the original method include the definition of the object's center as the same point before and after strain (Dunne et al., 1990) and the non-elliptical shapes of some objects (Mulchrone and Roy Choudhury, 2004). Our data sets are smaller than ideal but the central void is a well-defined ellipse (Fig. 8) and the order of magnitude of the strain ellipse is obtained even if the first decimal place is ±0.5. Normalized Fry analysis improves the method where objects do not have equal initial size (Erslev, 1988; Erslev and Ge, 1990). However, automated fitting of an ellipse through normalized data may be affected by elliptical concentrations that are not the same axial ratio or orientation as the central void. We therefore used a manual ellipse-fitting process that starts with the largest circle that fits inside all the data and then extends one radius of the circle to become the long axis of the best-fit ellipse. By trial and error, the longest possible long axis direction is discovered. Subsequent to our submission of this paper, Waldron and Wallace (2007) suggested an objective ellipse-fitting procedure based on the original annulus concept in Crespi (1986). This is worth considering for future work.

After hand-fitting ellipses on Fry plots, the program calculated the orientation (Phi) and $R_s$ (axial ratio) for each strain ellipse (Fig. 8). $R_s$ values were used to calculate the elongation (negative values= shortening):

$$e = \frac{l_f - l_i}{l_i} \tag{1}$$

where $e$ is elongation (or shortening if values are negative), $l_f$ is the deformed (final) axial length and $l_i$ is the undeformed (initial) axial length. If the undeformed length is the radius ($r$) of a circle that has an area equal to an ellipse with axial ratio $R_s = \frac{a}{b}$ (where $a$ is the longest, and $b$ the shortest axis), then the area of the circle $(A) = \pi \times r^2$ (where $r = l_i$) and the area of the ellipse $(A) = \pi \times a \times b$ (where $b = l_f$).

Thus,

$$l_i^2 = a \times l_f \tag{2}$$

By substituting Eq. (2) into Eq. (1) we obtain:

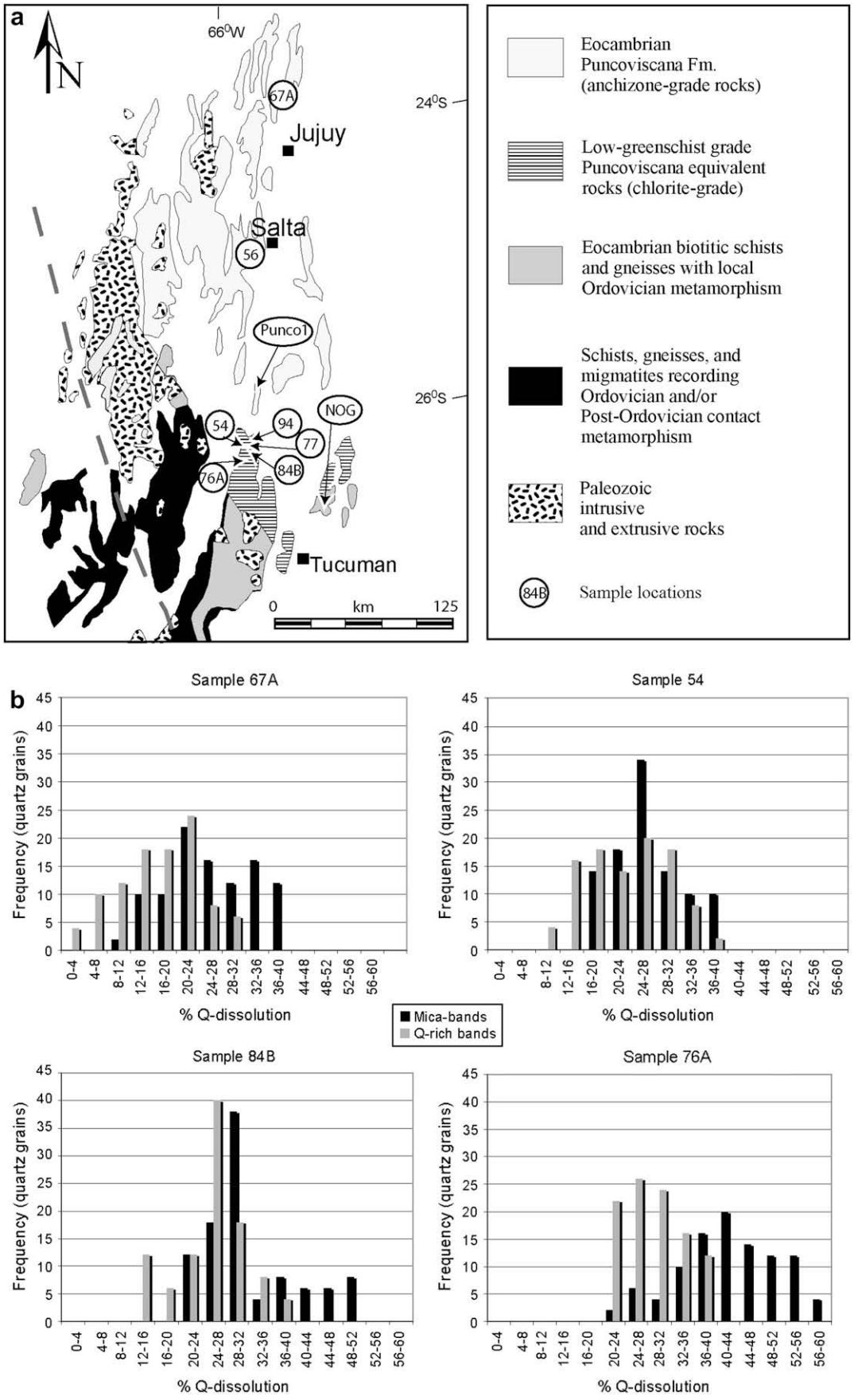


**Fig. 7.** (a) Simplified geological map of Lower Paleozoic rocks in NW Argentina, modified from Willner and Miller (1985), Becchio and Lucassen (2002), and Simpson et al. (2003) with the location of the samples mentioned in the text and samples used for quartz-dissolution calculations and Fry analysis. (b) Frequency histograms showing quartz dissolution % distribution in 4 samples with increasing metamorphic grade.

**Table 1**
Summary of percentage quartz dissolution averages and standard deviations of four samples (location shown in Fig. 7a) listed from left to right in order of increasing inferred depth and metamorphic grade

| Sample | 67A | 54 | 84B | 76A |
|---|---|---|---|---|
| Q-dissolution in mica-rich bands | 25.9 ± 7.7 | 26.8 ± 5.5 | 32.14 ± 8 | 42.3 ± 8.6 |
| Q-dissolution in Q-rich bands | 16.7 ± 7.1 | 23.1 ± 6.9 | 25.3 ± 6.2 | 28.9 ± 5.1 |

$$e = \sqrt{\frac{1}{R_s}} - 1 \quad (3)$$

which can be directly used to calculate rock shortening with the obtained $R_s$ values. The six values of Phi, $R_s$, and shortening obtained for each thin section were averaged to obtain an average Phi, $R_s$, and shortening value for each sample (Table 2).

Finite strain ellipse orientations range from ~20° to ~47° to bedding. The average Phi value for the anchizone-grade sample 67A is greater than for samples at higher metamorphic grade; with increasing grade, the finite strain ellipse tends to be at a lower angle with respect to $S_P$ (Table 2). There are minor differences in shortening values in thin sections cut parallel and perpendicular to strike (samples AP-94A1 and AP-94A2 show 30.33% and 30.93% shortening respectively, whereas samples 77A and 77B have shortening values of 30.31% and 29.92% respectively). Average strain magnitudes generally increase with metamorphic grade, and range from ~21% shortening in the anchizone sample, to ~33% shortening in greenschist facies samples, with most recording ~30%. Thus, a high Phi value (~46°) and a relatively low strain magnitude (~21% shortening) characterize the lowest grade (shallowest) sample, whereas smaller Phi values (mean ~27°) and higher-strain magnitudes (mean ~30% shortening) are recorded by higher grade (deeper) samples. These calculations involve the assumption that clasts and matrix experienced the same strain. This simplification underestimates shortening, as some greywackes contain up to 20% matrix (Appendices A and B).

**Table 2**
Data from Fry analysis obtained from seven samples listed in order of inferred depth and metamorphic grade (location of samples shown in Fig. 7a)

| Sample | Phi | $R_s$ | Shortening | Sample | Phi | $R_s$ | Shortening |
|---|---|---|---|---|---|---|---|
| 67A | 40.00 | 1.72 | −23.75 | 77A | 19.00 | 1.99 | −29.11 |
| | 51.00 | 1.46 | −17.24 | | 16.00 | 2.01 | −29.47 |
| | 46.00 | 1.61 | −21.19 | | 15.00 | 1.88 | −27.07 |
| | 59.00 | 1.59 | −20.69 | | 31.00 | 2.36 | −34.91 |
| | 36.00 | 1.57 | −20.19 | | 16.00 | 2.12 | −31.32 |
| | 48.00 | 1.57 | −20.19 | | 26.00 | 2.04 | −29.99 |
| Average | 46.67 | 1.59 | −20.54 | Average | 20.50 | 2.07 | −30.31 |
| 54 | 29.00 | 1.70 | −23.30 | 77B | 32.00 | 1.95 | −28.39 |
| | 41.00 | 1.93 | −28.02 | | 19.00 | 1.96 | −28.57 |
| | 41.00 | 1.64 | −21.91 | | 29.00 | 1.99 | −29.11 |
| | 41.00 | 1.77 | −24.84 | | 17.00 | 2.15 | −31.80 |
| | 23.00 | 1.81 | −25.67 | | 24.00 | 1.90 | −27.45 |
| | 39.00 | 1.47 | −17.52 | | 34.00 | 2.31 | −34.20 |
| Average | 35.67 | 1.72 | −23.54 | Average | 25.83 | 2.04 | −29.92 |
| 84B | 26.00 | 1.87 | −26.87 | 76A | 31.00 | 2.37 | −35.04 |
| | 24.00 | 2.58 | −37.74 | | 21.00 | 2.39 | −35.32 |
| | 30.00 | 1.99 | −29.11 | | 40.00 | 2.45 | −36.11 |
| | 34.00 | 2.11 | −31.16 | | 37.00 | 1.89 | −27.26 |
| | 45.00 | 2.01 | −29.47 | Average | 32.25 | 2.8 | −33.43 |
| | 41.00 | 1.94 | −28.20 | | | | |
| Average | 33.33 | 2.08 | −30.43 | | | | |
| AP-94A1 | 33.00 | 2.00 | −29.29 | NOG | 21 | 2.43 | −35.85 |
| | 29.00 | 2.44 | −35.98 | | 20 | 2.38 | −35.18 |
| | 39.00 | 1.67 | −22.62 | | 11 | 2.35 | −34.77 |
| | 5.00 | 2.12 | −31.32 | | 36 | 1.77 | −24.84 |
| | 17.00 | 2.01 | −29.47 | | 19 | 2.33 | −34.49 |
| | 11.00 | 2.25 | −33.33 | | 10 | 2.53 | −37.13 |
| Average | 22.33 | 2.08 | −30.33 | Average | 19.50 | 2.30 | −33.71 |
| AP-94A2 | 43.00 | 1.90 | −27.45 | | | | |
| | 8.00 | 2.36 | −34.91 | | | | |
| | 22.00 | 1.80 | −25.46 | | | | |
| | 36.00 | 2.39 | −35.32 | | | | |
| | 39.00 | 2.16 | −31.96 | | | | |
| | 26.00 | 2.07 | −30.50 | | | | |
| Average | 29.00 | 2.11 | −30.93 | | | | |

Samples 67A, 54, 84B, and 76A were out perpendicular to bedding and normal to fold hinges (or parallel to the mineral lineation where present). Sections AP-94A1 and AP-94A2 are mutually perpendicular (parallel and perpendicular to lineation respectively). Sections 77A (parallel to lineation) and 77B (perpendicular to lineation) are also mutually perpendicular Phi is the orientation of the long axis, measured counterclockwise from a horizontal reference line ($S_p$). $R_s$ is the ratio of long to short axes. Percent shortening was calculated from $R_s$ values.

## 7. Discussion

Primary sedimentary features are still identifiable in many of the metamorphosed siliciclastic sediments of the Sierras Pampeanas. In the low-grade Puncoviscana Formation rocks (mid to upper anchizone; Toselli and Weber, 1982; Do Campo and Omarini, 1990; Do Campo et al., 1994), the composition of the relatively quartz-rich beds described here is typical of immature greywackes and the locally graded, quartz-rich beds capped with clay-rich laminae, are typical of turbiditic deposits (Jezek et al., 1985). Numerous relict sedimentary structures, such as cross-bedding, lenticular bedding, slumps, graded bedding, dewatering structures, and flame structures, are preserved in banded psammites that are the low-grade metamorphic equivalents of the Puncoviscana Formation and enable a clear distinction to be drawn between pre- and post-folding foliation development.

### 7.1. Development of pre-tectonic foliation ($S_P$)

In the least metamorphosed rocks of the Puncoviscana Formation, the presence of numerous elongate and apparently strain-free quartz grains that have truncated borders parallel to bedding, pressure shadows, and bedding-parallel seams of insoluble residues, indicate that pressure-solution was active as a deformation mechanism. Compaction-related pressure-solution demonstrably enhanced primary quartz-rich and quartz-poor bands by facilitating the removal of quartz from clay-rich sedimentary layers well before the superposition of chevron folds ($F_1$) with their related tectonic cleavage ($S_1$). Grain area analyses show that with increase in metamorphic grade (or structural depth), dissolution of quartz in mica-rich domains increased significantly, with an associated increase in metamorphic mica and chlorite content. Quartz grains have highly dissolved borders in contact with mica grains, and have high axial ratios in mica-rich bands in contrast to lower axial ratios in quartz-rich bands. Significant quartz loss in mica-rich bands, with a concomitant passive increase in mica content, is consistent with phyllosilicate-enhanced dissolution as proposed by Engelder and Marshak (1985), Marshak and Engelder (1985), Hickman and Evans (1995), Farver and Yund (1999), and Renard et al. (2001), among others. An increase in quartz grain dissolution along with an increase in abundance of solution seams parallel to bedding, and more abundant phyllosilicate mica beards, are all consistent with pressure-solution and, to a lesser degree, neo-crystallization processes, becoming more prevalent with increasing metamorphic grade.

We propose that the original sedimentary clay-rich laminae, parallel or subparallel to bedding, acted to localize subsequent cleavage-seam nucleation and propagation (see also Gregg, 1985; Schweitzer and Simpson, 1986; Tapp and Wickham, 1987; Yang and Gray, 1994; Fueten et al., 2002). As a result, disjunctive cleavage planes, $S_p$, formed normal to the shortening direction, which in these rocks was also initially normal to bedding (Fig. 9a). We relate the $S_p$ disjunctive cleavage to the initial compositional

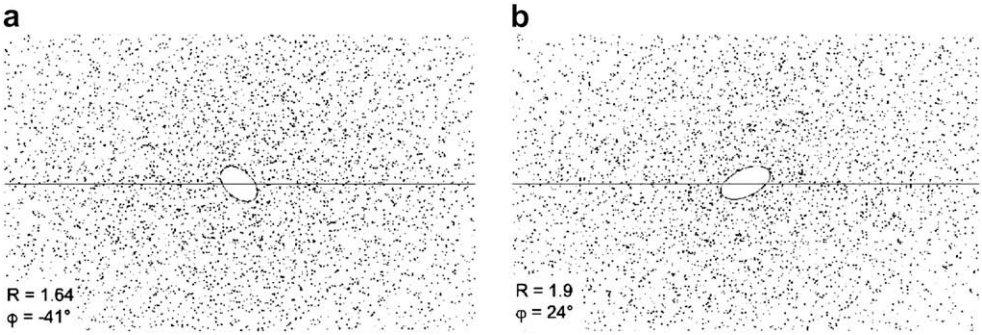


**Fig. 8.** Representative Fry diagrams from selected samples of chlorite-grade banded psammites. Diagrams include a hand-fitted ellipse and calculated orientation (Phi) and axial ratio ($R$ or $R_s$ in the text) for each strain ellipse. (a) Fry plot of a thin section from sample 54; $n = 80$. (b) Fry plot of a thin section from sample 77B; $n = 75$.

heterogeneity of the turbiditic rocks, rather than calling upon special circumstances such as dewatering channels (e.g., Gray, 1978) or bioturbation (e.g., Nickelsen, 1972). During the post-diagenetic anchizone metamorphism, recrystallization of the original clay minerals formed small white micas and chlorite, all oriented parallel to bedding. Increasing depth and temperature to greenschist facies conditions produced the univariant assemblage Chl + Plag or the assemblage, Qtz + Kfs + Bt + Ms + Pl(Ab); neo-crystallization and recrystallization became more important in clay/mica-rich bands, as shown by the progressive increase in grain size of metamorphic chlorite, white mica, muscovite, and biotite.

The presence of quartz overgrowths parallel to bedding suggests that part of the silica mobilized from the mica-rich bands could have been reprecipitated in the nearby quartz-rich bands. Higher volume loss in mica-rich bands is consistent with mica-grains acting as stress concentrators to shelter adjacent quartz-rich zones from deformation and therefore from quartz dissolution, as suggested by Fueten et al. (2002).

The initial amount of clay/phyllosilicates and their sedimentary distribution/arrangement initially present in the rock will determine cleavage spacing (Fueten et al., 2002) and the amount of silica that can be locally mobilized from one area of the rock to another. Thus in our conceptual model (Fig. 9a), the original clay- and chlorite-rich sedimentary laminae of the Puncoviscana Formation preferentially developed a disjunctive cleavage parallel to bedding, $S_p$, in anchizone rocks and became further transformed at greenschist facies into alternating quartz-poor and quartz-rich compositional banding, similar in appearance to the classic P-Q fabrics of Waldron and Sandiford (1988), the 'type C' rough cleavage defined by Gray (1978) and Onasch (1983), and the zonal cleavage described by Murphy (1990). Our results support the model of Fueten et al. (2002) in which disjunctive cleavage can develop as a result of rheological instability in a rock, which in our examples is an initial, relatively regularly spaced compositional variation.

### 7.2. Development of tectonic cleavage ($S_1$)

The first recorded tectonic event in the Puncoviscana Formation and related turbiditic rocks folded bedding and $S_p$ into the ubiquitous, decameter-scale, upright $F_1$ chevron folds that characterize the Pampean deformation of the region (Fig. 9b). In anchizone to low greenschist facies rocks, $S_1$ cleavage on $F_1$ chevron fold limbs cross-cuts both $S_p$ and intra-bed sedimentary structures such as slumps and cross-bedding at angles from 15° to as high as 45°. Therefore, $S_p$ developed prior to $F_1$ (Fig. 9b). Sedimentary slump folds that are preserved in low-grade, quartz-rich, centimeter-scale turbiditic beds have no geometrical relationship to the $F_1$ chevron folds. In rocks that reached biotite grade, in which no identifiable intra-bed sedimentary structures are preserved, the axial-planar $S_1$ cross-cuts relict $S_0$ bedding planes and $S_P$ compositional banding in fold hinges (Fig. 9b), again demonstrating that it postdates formation of the bands. However, $S_1$ enhances and may be indistinguishable from $S_p$ where the two foliations are subparallel on the limbs of tight folds.

In low-grade (anchizone) pelites and mica-rich domains in banded psammites, $S_1$ is defined by the uniform, syn-tectonic neo-crystallization of illite and small white micas. However, in adjacent metagreywackes with low mica content, $S_1$ did not develop. Therefore, the original clay/mica content of the rock seems to be a determining factor in the degree of cleavage development. In higher-grade (chlorite-grade) psammites, new micas at an angle of 30–45° with respect to $S_p$ suggest that $S_1$ formation was related to differential movement between compositional bands during flexural slip of the multilayered sequence. $S_1$ in these metasedimentary rocks is defined by sheared and recrystallized white mica grains, chlorite, and muscovite, and wraps around asymmetric quartz and feldspar grains. The later clasts exhibit pressure shadows, and truncated detrital grain boundaries where they abut pressure-solution seams, thereby serving to further enhance the compositional banding on fold limbs. Thus, in low greenschist facies $S_1$ cleavage domains on fold limbs, solution seams and quartz clasts with high axial ratios indicate that pressure-solution was still a dominant mechanism, with possibly some mica-sliding along cleavage planes in phyllosilicate-rich layers.

The distinctively biotite banded schists of Nogalito (Fig. 1) illustrate the transition from pressure-solution dominated $S_1$ foliation to the start of crystal-plastic dominated $S_1$ foliation. Elongated detrital quartz grains with undulatory extinction and pressure-solution seams parallel to the compositional banding are still preserved in these rocks. However, we also observe a quartz grain shape preferred orientation that is parallel to $S_1$ and oblique to $S_p$ on fold limbs and the presence of bulging quartz grain boundaries, consistent with Regime 1 (Hirth and Tullis, 1992) grain boundary migration recrystallization. Grains in fold hinges are more equant, which suggests that the original bedding-parallel pressure-solution foliation ($S_P$) was more enhanced on fold limbs than in the $F_1$ fold hinge regions. Deformation textures are consistent with syn-$F_1$ dynamic recrystallization at deformation temperatures of 250 ± 50 °C, somewhat lower than the equilibrium temperature indicated by the mineral assemblage present in these rocks (~400–425 °C at about 3.5 kbar; Mather, 1970; Miyashiro and Shido, 1985), which suggests that $F_1$ deformation continued after the peak of metamorphism.

In most biotite banded schists (e.g., Tafi del Valle, Ancasti; Fig. 1), new mica growth was the predominant mechanism for the formation of $S_1$, e.g., new micas in the limbs of crenulated $S_p$, or oriented large, tabular biotite grains parallel to $F_1$ axial planes. Changes from pressure-solution dominated foliations to those dominated by recrystallization-accommodated dislocation creep have been previously described from mid- to upper-greenschist facies rocks (e.g., Passchier and Trouw, 1996; Worley et al., 1997),

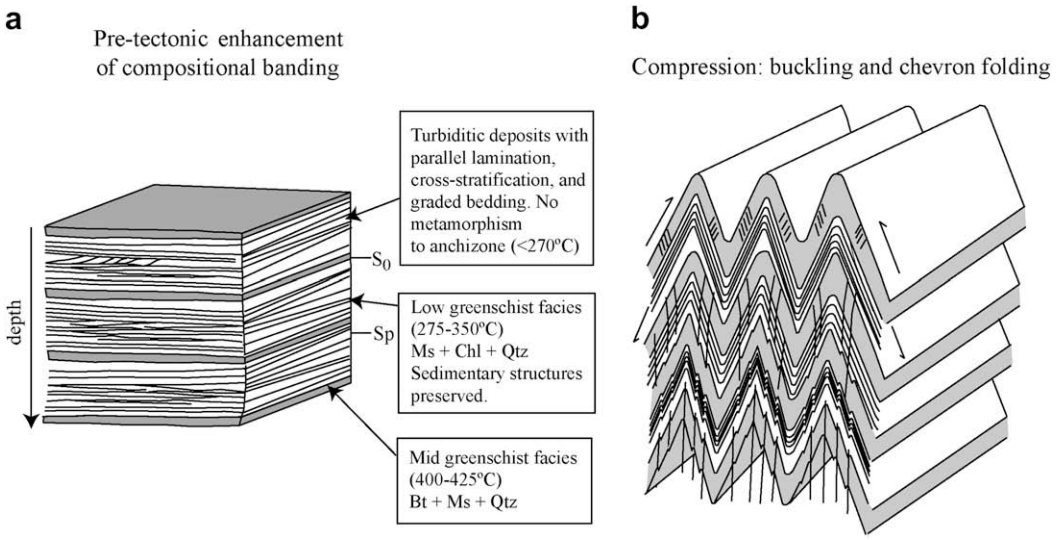


**Fig. 9.** Proposed model for development of $S_p$ and $S_1$. (a) Deposition and burial of turbidite deposits; with increasing depth (arrow), compaction-related processes align micas and pressure-solved quartz grains sub-parallel to bedding ($S_0$) to form $S_P$. (b) Later horizontal shortening above a buried detachment results in chevron folding with a fanning $S_1$ cleavage in pelitic layers at upper levels, a tight fan of $S_1$ in mid-level pelites and psammites, and an axial planar $S_1$ with local parasitic folds in deeper sections.

however the lack of quartz lattice-preferred orientations even in quartz-rich bands of the Nogalito schist precludes significant dislocation creep. Rather, the transition is directly from pressure-solution dominated deformation to incipient grain boundary migration deformation accompanied by new mica growth. Grain boundary migration processes with no lattice preferred orientation have been previously described in the literature (Smith et al., 2007).

### 7.3. Folding model

Truncated grain boundaries, pressure shadows, and seams of insoluble residues parallel to bedding are consistent with early compaction, which would have altered the geometry of sedimentary structures and permitted $S_p$ formation. The subsequent widespread, upright $F_1$ chevron folding is seen at all structural levels and records horizontal shortening. Slip on pre-existing sedimentary anisotropies, such as clay-rich layers and the enhanced $S_p$ foliation, may have occurred during the initial stages of $F_1$ deformation.

As the chevron folds tightened, bedding-parallel $S_p$ foliations in banded psammites were able to behave as centimeter-scale multilayered sequences. Previously formed and enhanced planar mica-rich bands would have a relatively low resistance to shear and thereby facilitate slip (e.g., Hoeppener, 1956; Ramsay, 1967; Dieterich, 1969; Engelder and Marshak, 1985). In the banded psammites, mica-rich domains would localize finite strain (e.g., Ramsay and Huber, 1987; Model 1 of Murphy, 1990), leading to the development of $S_1$ cleavage by mica and chlorite grain reorientation, and the enhancement of pressure-solution, as recorded by our volume loss data. In pelites, aligned and undeformed new micas indicate that oriented mineral growth occurred during the last stages of flexural slip. With progressive increase in metamorphic grade, rock ductility increased and parasitic folds developed along with the $S_1$ axial planar and disjunctive crenulation cleavage.

Bedding-perpendicular total strain magnitudes obtained from the Fry analyses are likely to be the product of both $S_p$ formation and $F_1$-related deformation. Possible sources of error in our estimates include grains that are not perfect ellipsoids, pressure-solution-modified grain shapes, and non-uniform initial particle distribution. Shortening values, which indicate the total strain in the rock, may be influenced by preferential grain alignment during the formation of primary structures, such as bedding planes and cross-beds. If this is the case, then we might be overestimating the total strain in non-metamorphosed sandstones or even greenschist-facies psammites where the sedimentary fabric is locally strong. Shortening strains may also be the result of minor crystal plasticity with or without grain boundary sliding, and pressure-solution during both compaction and later chevron folding.

## 8. Conclusions

Banded psammites contain a variety of fabrics whose origins depend largely on the initial composition and mineral arrangement of the sedimentary protolith. High finite strains are shown to have been localized in the less competent primary layers, which are inferred to develop into the mica-rich domains of banded psammites. Clay-rich bands acted as the loci for mica nucleation and growth, favoring dissolution of quartz and thereby passive concentration of mica. These processes generated a compaction-related cleavage ($S_P$), parallel everywhere to bedding that enhanced and mimicked the original sedimentary planar fabric ($S_0$). As a result, banded sandstones developed a disjunctive bedding-parallel cleavage at lower greenschist facies. With increasing metamorphic grade, which in these rocks can be equated to structural depth, pressure-solution and mica growth become increasingly important in mica-rich domains, thereby enhancing the disjunctive cleavage. These processes resulted in the formation of compositionally banded schists. Our observations suggest that: (1) the cleavage type and its morphology are determined by the pre-existing sedimentary fabric, particularly in the generation of disjunctive cleavage and (2) the formation of a compositional banding during metamorphism does not require tectonic transposition of an older tectonic foliation.

## Acknowledgements

This material is based upon work supported by the National Science Foundation under Grant EAR-0073852 to CS. Any opinions, findings, and conclusions expressed in this material are those of the authors and do not necessarily reflect the views of the National Science Foundation. The authors are grateful to D.G. DePaor, J.C. Escamilla-Casas, T. Plank, D.M. FitzGerald, J.P. Lopez, R. Miró, J.N. Rossi de Toselli, and A. Toselli, for helpful discussions at different stages of the work, and to Laurel Goodwin and an anonymous reviewer for their thoughtful and constructive reviews.

## Appendix A

**Table A.1**
Metamorphic grade, thickness of the compositional banding, and petrographic description of the samples mentioned in the text (location of samples shown in Fig. 7a)

| Sample (Massive Greywackes) | Metamorphic grade | | Matrix % | Matrix composition | Clast composition | | Accessory minerals |
|---|---|---|---|---|---|---|---|
| 56 | Anchizone | | 15 | Ill, Qtz, Chl, small white micas | Qtz, Pl, Kfs, lithics (pelites quartzites, chert), iron oxides | | Tourmaline, zircon, iron oxides |
| Punco 1 | Anchizone | | 20–25 | Ill, Qtz, Chl, small white micas | Qtz, Pl, Kfs, lithics (pelites quartzites, chert) | | Zircon, tourmaline, iron oxide, carbonate |
| Sample (banded sandstones/ banded psammites) | Metamorphic grade | Thickness of the compositional banding | Matrix % in the quartz-rich bands | Matrix composition | Quartz-rich bands clast composition | Mica-rich bands composition | Accessory minerals |
| 67A | Anchizone | 1/2 cm mica-rich bands; 2 cm quartz-rich bands | 20 | Ill, Qtz, Chl | Qtz, Pl, Kfs, lithics (pelites quartzites, chert) | Ill, small white micas, Ms, Qtz, Kfs, lithics | Iron oxides, zircon |
| 54 | Chlorite grade | 1/2 cm mica-rich bands; 1.5 cm quartz-rich bands | 15 | Ill, Qtz, Chl | Qtz, Pl, Kfs, scarce lithics (quartzite) | Ms, Chl, Ill, Qtz, Kfs, lithics | Zircon, tourmaline, iron oxides |
| 84B | Chlorite grade | 0.25–0.5 cm mica-rich bands; 0.5 cm quartz-rich bands | 10–15 | Ill, Qtz, Chl, small white micas | Qtz, Kfs, Pl, few pelite and quartzite clasts | Ms, Chl, Ill, Qtz, Kfs, lithics | Zircon, sphene, tourmaline iron oxides |
| AP-94A1 | Chlorite grade | 0.2 cm mica-rich bands; 0.8 cm quartz-rich bands | 10 | Ill, Qtz, Chl, small white micas | Qtz, Kfs, Pl, few quartzite clasts | Ms, Chl, Qtz, Kfs, few lithics | Sphene, zircon, tourmaline carbonate |
| AP-94A2 | Chlorite grade | 0.2 cm mica-rich bands; 0.8 cm quartz-rich bands | 10 | Ill, Qtz, Chl, small white micas | Qtz, Kfs, Pl, few quartzite clasts | Ms, Chl, Qtz, Kfs, fw lithics | Sphene, zircon, tourmaline carbonate |
| 77A | Chlorite grade | 0.3–0.5 cm mica-rich bands; 1 cm quartz-rich bands | 10, some recrystallization | Ill, Qtz, Chl, Ms | Qtz, Kfs, Pl, very few quartzite clasts | Ms, Chl, Qtz, Kfs | Zircon, tourmaline, iron oxides |
| 77B | Chlorite grade | 0.3–0.5 cm mica-rich bands; 1 cm quartz-rich bands | 10, some recrystallization | Ill, Qtz, Chl, Ms | Qtz, Kfs, Pl, very few quartzite clasts | Ms, Chl, Qtz, Kfs | Zircon, tourmaline, iron oxides |
| 76A | Chlorite grade | 0.4 cm mica-rich bands; 0.8 cm quartz-rich bands | 10, some recrystallization | Ill, Qtz, Chl, Ms | Qtz, Kfs, Pl, some lithic fragments of quartzite | Ms, Chl, Qtz, Kfs, few Bt grains | Zircon, tourmaline, iron oxides |
| Nogalito | Biotite grade | 0.1–0.2 cm mica-rich bands; 0.4 cm quartz-rich bands | 0 | | Qtz, Kfs, Pl, some lithic fragments of quartzite | Ms, Chl, Bt, Qtz, Kfs, few lithics | Zircon, tourmaline, iron oxides |

## Appendix B

**Table B.1**
Estimated percentage of minerals, matrix, and different types of lithic clasts in thin section from the samples mentioned in the text (location of samples shown in Fig. 7a)

| | 67A | 56 | Punco 1 | 54 | 84B | AP-94A1 | AP-94A2 | 77A | 77B | 76A | Nogalito |
|---|---|---|---|---|---|---|---|---|---|---|---|
| Qtz | 35 | 35 | 38 | 40 | 50 | 55 | 55 | 50 | 50 | 52 | 60 |
| Kfs | 7 | 10 | 10 | 17 | 12 | 10 | 10 | 10 | 10 | 9.5 | 15 |
| Pl | 5 | 7 | 3 | 5 | 7 | 4 | 4 | 5 | 5 | 3 | 5 |
| Ill/Ms/Chl | 10 | 10 | 15 | 15 | 10 | 12 | 12 | 15 | 15 | 15 | 3 |
| Bt | 0 | 0 | 0 | 0 | 0 | 0 | 0 | 0 | 0 | 0-% | 12 |
| *Lithic fragments %* | | | | | | | | | | | |
| Pelites | 13 | 6 | 5 | 3 | 3 | 2 | 2 | 0 | 0 | 0 | 0 |
| Quartzite | 5 | 7 | 3 | 5 | 3 | 5 | 5 | 7 | 7 | 8 | 5 |
| Chert | 5 | 10 | 6 | 0 | 5 | 2 | 2 | 3 | 3 | 2 | 0 |
| matrix | 20 | 15 | 20 | 15 | 10 | 10 | 10 | 10 | 10 | 10 | 0 |

## Appendix C

**Table C.1**
Whole-rock ICP–MS analyses of banded quartzites. Sample 67A is in the anchizone grade, and samples 94 and 77 are in the chlorite grade (locations in Fig. 7a). Sample 63TURB is a chlorite-grade banded psammite from Vipos and 9846-2 is a biotite banded schist from Tuclame (localities in Fig. 7a).

| | 67A | 94 | 77 | 63TURB | 9846-2 |
|---|---|---|---|---|---|
| $SiO_2$ | 74.40 | 77.26 | 76.24 | 77.15 | 77.75 |
| $TiO_2$ | 0.88 | 0.60 | 0.70 | 0.54 | 0.50 |
| $Al_2O_3$ | 11.19 | 11.02 | 10.55 | 11.41 | 11.31 |
| $Fe_2O_3$ | 5.00 | 4.02 | 3.93 | 2.70 | 3.76 |
| MgO | 1.68 | 2.21 | 1.83 | 1.22 | 1.69 |
| MnO | 0.07 | 0.07 | 0.05 | 0.05 | 0.06 |
| CaO | 0.52 | 1.44 | 0.39 | 1.71 | 0.97 |
| $K_2O$ | 1.96 | 1.40 | 1.40 | 2.40 | 2.73 |
| $Na_2O$ | 2.25 | 2.16 | 2.91 | 2.75 | 1.76 |
| $P_2O_5$ | 0.19 | 0.16 | 0.19 | 0.15 | 0.12 |
| Total | 98.14 | 100.34 | 98.19 | 100.09 | 100.65 |
| Sc | 10.31 | 8.74 | 8.40 | 7.75 | 7.41 |
| Y | .31.15 | 25.06 | 29.76 | 25.91 | 23.11 |
| Ba | 232.04 | 210.68 | 247.35 | 306.65 | 286.21 |

All Fe analyzed as $Fe_2O_3$.

## References


Adams, C., Miller, H., Toselli, A., 1990. Nuevas edades de metamorfismo por el método K-Ar de la Formación Puncoviscana y equivalentes, NW de Argentina. In: Aceñolaza, F.G., Miller, H., Toselli, A.J. (Eds.), El Ciclo Pampeano en el Noroeste Argentino, Serie Correlación Geológica, 4. Universidad Nacional de Tucumán, San Miguel de Tucumán, pp. 209–219.

Aceñolaza, F.G., 1978. El Paleozóico inferior de Argentina segun sus trazas fósiles. Ameghiniana 15, 15–64.

Aceñolaza, G.F., 2004. Precambrian-Cambrian ichnofossils, an enigmatic 'annelid tube' and microbial activity in the Puncoviscana Formation (La Higuera; Tucuman Province, NW Argentina). Geobios 37, 127–133.

Aceñolaza, F.G., Aceñolaza, G.F., 2007. Insights in the Neoproterozoic Early Cambrian Transition of NW Argentina: Facies, Environments and Fossils in the Proto-margin of Western Gondwana. In: Special Publications, vol. 286. Geological Society, London, pp. 1-13.

Aceñolaza, F.G., Durand, F.R., 1986. Upper Precambrian-Lower Cambrian biota from the Northeast of Argentina. Geological Magazine 123, 367–375.

Aceñolaza, F.G., Miller, H., Toselli, A., 1988. The Puncoviscana Formation (Late Precambrian–Early Cambrian): Sedimentology, Tectonometamorphic history and age of the oldest rocks of the NW Argentina. Lecture Notes in Earth Sciences 17, 25–37.

Banks, C.J., Winchester, J.A., 2004. Sedimentology and stratigraphic affinities of Neoproterozoic coarse clastic successions, Glenshirra Group, Inverness-shire, Scotland. Scottish Journal of Geology 40, 159–174.

Becchio, R., Lucassen, F., 2002. Concordant titanite U–Pb ages of Cambrian to Silurian high T metamorphism at the western edge of Gondwana (Southern Puna and Western Sierras Pampeanas, Argentina, 26–29°). In: Andean Geodynamics, Extended Abstracts, 5th International Symposium Toulouse, France, pp. 77–80.

Borradaile, G.J., Bayly, M.B., Powell, C.M.A., 1982. Atlas of Deformational and Metamorphic Rock Fabrics. Springer-Verlag, Berlin, Heidelberg, New York.

Boyer, S.E., 1984. Origin and significance of compositional layering in late Precambrian Sediments Blue Ridge province, North Carolina USA. Journal of Structural Geology 6, 121–133.

Crespi, J.M., 1986. Some guidelines for the practical application of Fry's method of strain analysis. Journal of Structural Geology 8, 799–808.

Davidson, A., 1984. Identification of ductile shear zones in the southwestern Grenville Province of the Canadian Shield. In: Kroner, A., Greiling, R. (Eds.), Precambrian Tectonics Illustrated. Schweitz Verlag, Stuttgart, pp. 207–235.

De Paor, D.G., 1989. An interactive program for doing Fry Analysis on the Macintosh microcomputer. Journal Geological Education 37, 171–180.

De Paor, D.G., 2001. Structural Analysis: An On-line Course and CD ROM. Chapter 11, 2D methods – Fry, http://users.wpi.edu/~declan/Structural_Analysis/index.swf

Dennis, J.B., 1972. Structural Geology. Ronald Press, New York.

Dieterich, J.H., 1969. Origin of cleavage in folded rocks. American Journal of Science 267, 155–165.

Do Campo, M., Omarini, R., 1990. Contribucion al estudio de la evolucion diagenetica de la Formacion Puncoviscana en la Provincia de Salta, Argentina, Actas XI Congreso Geologico Argentino, vol. 2, pp. 161–164.

Do Campo, M., Nieto, F., 2003. Transmission electron microscopy study of very low-grade metamorphic evolution in Neoproterozoic pelites of the Puncoviscana Formation (Cordillera Oriental, NW Argentina). Clay Minerals 38, 459–481.

Do Campo, M., Omarini, R., Ostera, H., 1994. Edades K–Ar en fracciones finas de pelitas en la Formacion Puncoviscana Argentina. Revista Geologica de Chile 21, 233–240.

Do Campo, M., Nieto, F., Omarini, R., 1998. Mineralogía de las arcillas y metamorfismo de la Formación Puncoviscana en localidades de la Cordillera Oriental y Puna, Argentina. Actas X Congreso Latinoamericano de Geología, Buenos Aires, Argentina, pp. 217–223.

Do Campo, M., 1999. Metamorfismo del basamento en la Cordillera Oriental y borde oriental de la Puna. In: Gonzalez Bonorino, G., Omarini, R., Viramonte, J. (Eds.), Geologia del Noroeste de Argentina, XIV Congreso Geologico Argentino, Salta, Tomo I, Argentina.

Dunne, W.M., Onasch, C.M., Williams, R.T., 1990. The problem of strain-marker centers and the Fry method. Journal of Structural Geology 12, 933–938.

Durand, F.R., Aceñolaza, F.G., 1990. Caracteres biofaunísticos, paleoecológicos y paleogeográficos de la Formación Puncoviscana (Precámbrico superior-Cámbrico inferior) del Noroeste Argentino. In: Aceñolaza, F.G., Miller, H., Toselli, A.J. (Eds.), El Ciclo Pampeano en el Noroeste Argentino, Serie Correlación Geológica, 4. Universidad Nacional de Tucumán, San Miguel de Tucumán, pp. 71–112.

Engelder, T., Marshak, S., 1985. Disjunctive cleavage formed at shallow depths in sedimentary rock. Journal of Structural Geology 7, 327–343.

Erslev, E.A., 1988. Normalized center-to-center strain analysis of packed aggregates. Journal of Structural Geology 10, 201–209.

Erslev, E.A., Ge, H., 1990. Least-squares center-to-center and mean object ellipse fabric analysis. Journal of Structural Geology 12, 1047–1059.

Farver, J., Yund, R., 1999. Oxygen bulk diffusion measurements and TEM characterization of a natural ultramylonite: implications for fluid transport in mica-bearing rocks. Journal of Metamorphic Geology 17, 669–685.

Fry, N., 1979. Random point distributions and strain measurement in rocks. Tectonophysics 60, 89–105.

Fueten, F., Robin, P.Y., Schweinberger, M., 2002. Finite element modelling of the evolution of pressure solution cleavage. Journal of Structural Geology 24, 1055–1064.

Goodwin, L.B., Tikoff, B., 2002. Competency contrast, kinematics, and the development of foliations and lineations in the crust. Journal of Structural Geology 24, 1065–1085.

Gray, D.R., 1978. Cleavages in deformed psammitic rocks from Southeastern Australia: their nature and origin. Bulletin of the Geological Society of America 89, 577–590.

Gregg, W.J., 1985. Microscopic deformation mechanisms associated with mica film formation in cleaved psammitic rocks. Journal of Structural Geology 7, 45–56.

Hanna, S.S., Fry, N., 1979. A comparison of methods of strain determination in rocks from southwest Dyfed (Pembrokeshire) and adjacent areas. Journal of Structural Geology 1, 155–162.

Harper, C.T., Wolbaum, R.J., Thain, S., Senkow, M., Weber, D., Gunning, M., MacLachlan, K., 2002. Phelps Lake Project: geology and mineral potential of the Keseechewun Lake–Many Islands Lake area (parts of NTS 64M-9, -10, -15, and -16). In: Summary of Investigations 2. Saskatchewan Geological Survey, Saskatchewan Industry Resources.

Heldal, T., 2001. Ordovician stratigraphy in the western Helgeland Nappe Complex in the Brønnøysund area, North-central Norway. NGU-Bulletin 438, 47–61.

Hickman, S.H., Evans, E., 1995. Kinetics of pressure solution at halite-silica interfaces and intergranular clay films. Journal of Geophysical Research 100, 13113–13132.

Hirth, G., Tullis, J., 1992. Dislocation creep regimes in quartz aggregates. Journal of Structural Geology 14, 145–159.

Hoeppener, R., 1956. Zum Problem der Bruchbildung, Schieferung und Faltung. Geologische Rundschau 4, 247–283.

Hongn, F.D., Tubia, J.M., Aranguren, A., Mon, R., 2001. El batolito de Tástil (Salta, Argentina), un caso de magmatismo poliorogénico en el basamento andino. Boletín Geológico y Minero de España 112, 113–124.

ImageJ (formerly NIH Image): http://rsb.info.nih.gov/ij/

Jezek, P., 1986. Petrographie un fazies der Puncoviscana Formation, einer turbiditischen Folge im Jungprakambrium und Unterkambrium Nordwest-Argentiniens, PhD thesis, Westfalischen Wilhelms-Universitat Munster.

Jezek, P., 1990. Analisis sedimentológico de la Formación Puncoviscana entre Tucumán y Salta. In: Aceñolaza, F.G., Miller, H., Toselli, A.J. (Eds.), El Ciclo Pampeano en el Noroeste Argentino, 4. Universidad Nacional de Tucumán, San Miguel de Tucumán, pp. 9–36.

Jezek, P., Miller, H., 1987. Petrology and facies analysis of turbiditic sedimentary rocks of the Puncoviscana through (Upper Precambrian-Lower Cambrian) in the basement of the NW Argentine Andes. Gondwana Six: structure, tectonics, and geophysics. Geophysical Monograph 40, 287–293.

Jezek, P., Willner, A.P., Aceñolaza, F.G., Miller, H., 1985. The Puncoviscana trough – a large basin of Late Precambrian to Early Cambrian age on the pacific edge of the Brazilian shield. Geologische Rundschau 74, 573–584.

Jordan, P.G., 1988. The rheology of polymineralic rocks – an approach. Geologische Rundshau 77, 285–294.

Jordan, T.E., Allmendinger, R.W., 1986. The Sierras Pampeanas of Argentina: a modern analogue of Rocky Mountain foreland deformation. American Journal of Science 286, 737–764.

Keppie, J.D., Bahlburg, H., 1999. Puncoviscana formation of northwestern and central Argentina: passive margin or foreland basin deposit? In: Ramos, V.A., Keppie, J.D. (Eds.), Geological Society of America Special Paper. Geological Society of America, Boulder, Colorado, pp. 139–143.

Kretz, R., 1983. Symbols for rock-forming minerals. American Mineralogist 68, 277–279.

Kusky, T., De Paor, D.G., 1988. Strain analysis in rocks with a pre-tectonic fabric. Journal of Structural Geology 10, 529–530.

Lork, A., Miller, H., Kramm, U., Grauert, B., 1990. Sistemática U–Pb de circones detríticos de la Formación Puncoviscana y su significado para la edad máxima de sedimentación en la Sierra de Cachi (Provincia de Salta, Argentina). In: Aceñolaza, F.G., Miller, H., Toselli, A.J. (Eds.), El Ciclo Pampeano en el Noroeste

Argentino, 4, Serie Correlación Geológica. Universidad Nacional de Tucumán, San Miguel de Tucumán, pp. 199–208.
Marshak, S., Engelder, T., 1985. Development of cleavage in limestones of a fold and thrust belt in Eastern New York. Journal of Structural Geology 7, 345–359.
Mather, J.D., 1970. The biotite isograd and the lower greenschist facies in the Dalradian rocks of Scotland. Journal of Petrology 11, 253–275.
Maxwell, J.C., 1962. Origin of slaty and fracture cleavage in the Delaware Water Gap area, New Jersey and Pennsylvania. In: Engel, A.E.J., James, H.L., Leonard, B.F. (Eds.), Petrological Studies: A Volume in Honour of A.F. Buddington. Geological Society of America, Boulder, Colorado, pp. 281–311.
Means, W.D., 1975. Natural and experimental microstructures in deformed micaceous sandstones. Geological Society of America Bulletin 86, 1221–1229.
Meere, P.A., Mulchrone, K.F., 2003. The effect of sample size on geological strain estimation from passively deformed clastic sedimentary rocks. Journal of Structural Geology 25, 1587–1595.
Miyashiro, A., Shido, F., 1985. Tschermak substitution in low- and middle-grade pelitic schists. Journal of Petrology 26, 449–487.
Mulchrone, K.F., Roy Choudhury, K., 2004. Fitting an ellipse to an arbitrary shape: implications for strain analysis. Journal of Structural Geology 26, 143–153.
Murphy, F.X., 1990. The role of pressure solution and intermicrolithon-slip in the development of disjunctive cleavage domains: a study from Helvick Head in the Irish Variscides. Journal of Structural Geology 12, 69–81.
Nickelsen, R.P., 1972. Attributes of rock cleavage in some mudstones and limestones of the Valley and Ridge province, Pennsylvania. Pennsylvania Academy of Sciences Procedures 46, 107–112.
Omarini, R.H., 1983. Caracterizacion litologica, diferenciacion y genesis de la Formacion Puncoviscana entre el Valle de Lerma y la Faja Eruptiva de la Puna. PhD thesis(unpublished), Universidad Nacional. de Salta, Argentina.
Omarini, R.H., Baldis, B.A., 1984. Sedimentología y mecanismos deposicionales de la Formación Puncoviscana (Grupo Lerma, Precámbrico-Cámbrico) del norte argentino. In: IX Congreso Geológico de Argentina 1, pp. 383–398.
Omarini, R.H., Sureda, R.J., Gotze, H.J., Seilacher, A., Pfluger, F., 1999. Puncoviscana folded belt in northwestern Argentina: testimony of Late Proterozoic Rodinia fragmentation and pre-Gondwana collisional episodes. International Journal of Earth Sciences 88, 76–97.
Onasch, C.M., 1983. Origin and significance of microstructures in sandstones of the Martinsburg Formation. American Journal of Science 283, 936–966.
Onasch, C.M., 1990. Microstructures and their role in deformation of a quartz arenite from the central Appalachian foreland. Journal of Structural Geology 12, 883–894.
Pankhurst, R.J., Rapela, C.W., Saavedra, J., 1997. The Sierras Pampeanas of NW Argentina – growth of the Pre-Andean margin of Gondwana. European Union of Geosciences, Abstract Supplement 1, Terra Nova 9, 162.
Pankhurst, R.J., Rapela, C.W., Saavedra, J., Baldo, E., Dahlquist, J., Pascua, I., Fanning, C.M., 1998. The Famatinian magmatic arc in the central Sierras Pampeanas: an Early to Mid-Ordovician continental arc on the Gondwana margin. In: Pankhurst, R., Rapela, C. (Eds.), The Proto-Andean Margin of Gondwana. Special Publication 142. Geological Society, London, pp. 343–367.
Passchier, C.W., Trouw, R.A.J., 1996. Microtectonics. Springer, Berlin.
Powell, C.McA., 1979. A morphological classification of rock cleavage. In: Bell, T.H., Vernon, R.H. (Eds.), Microstructural processes during deformation and metamorphism. Tectonophysics, 58, pp. 21–34.
Powell, C.McA., 1984. Silurian to mid-Devonian—a dextral transtensional margin. In: Veevers, J.J. (Ed.), Phanerozoic Earth History of Australia. Clarendon Press, Oxford, pp. 309–329.
Piñán-Llamas, A., Simpson, C., 2006. Deformation of Gondwana margin turbidites during the Pampean orogeny, north-central Argentina. Geological Society of America Bulletin 118, 1270–1279.
Price, N.J., Cosgrove, J.W., 1990. Analysis of Geological Structures. Cambridge University Press, Cambridge.
Ramsay, J.G., 1967. Folding and Fracturing of Rocks. McGraw-Hill, New York, London.
Ramsay, J.G., Huber, M.I., 1983. Strain Analysis. In: The Techniques of Modern Structural Geology, vol. 1. Academic Press, London.
Ramsay, J.G., Huber, M.I., 1987. Folds and Fractures. In: The Techniques of Modern Structural Geology, vol. 2. Academic Press, London.
Rapela, C.W., Pankhurst, R.J., Casquet, C., Baldo, E.G., Saavedra, J., Galindo, C., 1998a. Early evolution of the Proto-Andean margin of South America. Geology 26, 707–710.
Rapela, C.W., Pankhurst, R.J., Casquet, C., Baldo, E.G., Saavedra, J., Galindo, C., Fanning, C.M., 1998b. The Pampean Orogeny of the southern proto-Andes: Cambrian continental collision in the Sierras de Córdoba. In: Pankhurst, R., Rapela, C. (Eds.), The Proto-Andean Margin of Gondwana. Special Publication 142. Geological Society, London, pp. 181–217.
Renard, F., Dysthe, D.K., Feder, J., Bjørlykke, K., Jamtveit, B., 2001. Enhanced pressure solution creep rates induced by clay particles: experimental evidence from salt aggregate. Geophysical Research Letters 28, 1295–1298.
Rosenberg, C., Stünitz, H., 2003. Deformation and recrystallization of plagioclase along a temperature gradient: an example from the Bergell tonalite. Journal of Structural Geology 25, 389–408.
Rossi de Toselli, J.N., Toselli, A., Durand, F.R., 1992. Metamorfismo de baja presión, su relación con el desarrollo de la cuenca Puncoviscana, plutonismo y régimen tectónico, Argentina. Estudios Geológicos 48, 279–287.
Roy, A.B., 1978. Evolution of slaty cleavage in relation to diagenesis and metamorphism: a study from the Hunsruckschiefer. Geological Society of America Bulletin 89, 1775–1785.
Saavedra, J., Toselli, A., Rossi, J., Pellitero, E., Durand, F., 1998. The Early Paleozoic magmatic record of the Famatina System: a review. In: Pankhurst, R., Rapela, C. (Eds.), The Proto-Andean Margin of Gondwana. Special Publication 142. Geological Society, London, pp. 283–295.
Schwartz, J.J., Gromet, L.P., 2004. Provenance of a late Proterozoic-early Cambria basin, Sierras de Córdoba, Argentina. Precambrian Research 129, 1–21.
Schweitzer, J., Simpson, C., 1986. Cleavage development in Elbrook Dolomite, SW Virginia. Geological Society of America Bulletin 97, 778–786.
Simpson, C., Whitmeyer, S., De Paor, D.G., Gromet, L.P., Miró, R., Krol, M.A., Short, H., 2001. Sequential ductile through brittle reactivation of major fault zones along the accretionary margin of Gondwana in Central Argentina. In: Holdsworth, R., Knipe, R.J., Strachan, R.A., Magloughlin, J. (Eds.), The Nature and Tectonic Significance of Fault Zone Weakening. Special Publication 186. Geological Society, London, pp. 233–255.
Simpson, C., Law, R.D., Gromet, P., Miró, R., Northrup, C.J., 2003. Paleozoic deformation in the Sierras de Córdoba and Sierra de las Minas, Eastern Sierras Pampeanas, Argentina. Journal of South American Earth Sciences 15, 749–764.
Sims, J.P., Ireland, T.R., Camacho, A., Lyons, P., Pieters, P.E., Skirrow, R.G., Stuart-Smith, P.G., Miró, R., 1998. U–Pb, Th–Pb and Ar–Ar geochronology from the southern Sierras Pampeanas, Argentina: implications for the Palaeozoic tectonic evolution of the western Gondwana margin. In: Pankhurst, R.J., Rapela, C.W. (Eds.), The Proto-Andean Margin of Gondwana. Special Publication 142. Geological Society, London, pp. 259–281.
Smith, S.A.F., Strachan, R.A., Holdsworth, R.E., 2007. Microstructural evolution within a partitioned microcrustal transpression zone, northeast Greenland Caledonides. Tectonics 26, doi:10.1029/2006TC001952.
Stallard, A., Shelley, D., 2005. The initiation and development of metamorphic foliation in the Otago Schist, Part 1: competitive oriented growth of white mica. Journal of Metamorphic Geology 23, 425–442.
Stallard, A., Shelley, D., Reddy, S., 2005. The initiation and development of metamorphic foliation in the Otago Schist. Part 2: evidence from quartz grain-shape data. Journal of Metamorphic Geology 23, 443–459.
Starkey, J., 2002. Chemical changes and the development of quartz preferred orientation in zones of crenulation cleavage, Anglesey. Journal of Structural Geology 24, 1627–1632.
Stipp, M., Stunitz, H., Heilbronner, R., Schmid, S.M., 2002a. The eastern Tonale fault zone: a 'natural laboratory' for crystal plastic deformation of quartz over a temperature range from 250 to 700 °C. Journal of Structural Geology 24, 1861–1884.
Stipp, M., Stünitz, H., Heilbronner, R., Schmid, S.M., 2002b. Dynamic Recrystallization of quartz: correlation between natural and experimental conditions. In: de Meer, S., Drury, M.R., de Bresser, J.H.P., Pennock, G.M. (Eds.), Deformation Mechanisms, Rheology and Tectonics: Current Status and Future Perspectives. Special Publication 200. Geological Society, London, pp. 171–190.
Tapp, B., Wickham, J., 1987. Relationships of rock cleavage fabrics to incremental and accumulated strain in the Conococheague Formation, USA. Journal of Structural Geology 9, 457–472.
Toselli, A., Weber, K., 1982. Anquimetamorfismo en rocas del Paleozóico inferior en el noroeste de Argentina. Valor de la cristalinidad de la illita como índice. Acta Geológica Lilloana 16, 187–200.
Toselli, A., Rossi de Toselli, J.N., 1982. Metamorfismo de la Formacion Puncoviscana en las provincias de Salta y Tucuman, Argentina, Quinto Congreso Latinoamericano de Geologia Actas II, pp. 37–52.
Toselli, A., 1990. Metamorfismo del Ciclo Pampeano. In: Aceñolaza, F.G., Miller, H., Toselli, A.J. (Eds.), El Ciclo Pampeano en el Noroeste Argentino, 4. Universidad Nacional de Tucumán, San Miguel de Tucumán, pp. 181–197.
Toselli, A., Rossi de Toselli, J.N., 1983. Controles del metamorfismo y deformacion en las parametamorfitas de las Cumbres de San Javier, Tucuman. Revista de la Asociación Geológica Argentina 38, 137–147.
Toselli, A., Rossi de Toselli, J.N., 1984. Metamorfismo de las Cumbres Calchaquíes: II Petrología del basamento esquistoso entre La Angostura y Tafí del Valle, Tucumán. Revista de la Asociación Geológica Argentina 39, 262–275.
Turner, J.C.M., 1960. Estratigrafía de la Sierra de Santa Victoria, 49. Academia Nacional de Ciencias de Córdoba, Argentina. 163–196.
Turner, J.C.M., Mon, R., 1979. Cordillera oriental, Segundo Simposio Regional de Argentina. Academia Nacional de Ciencias, Cordoba, pp. 57-94.
Waldron, H.M., Sandiford, M., 1988. Deformation volume and cleavage development in metasedimentary rocks from the Ballarat slate belt. Journal of Structural Geology 10, 53–62.
Waldron, J.W.F., Wallace, K.D., 2007. Objective fitting of ellipses in the centre-to-centre (Fry) method of strain analysis. Journal of Structural Geology 29, 1430–1444.
Whitmeyer, S.J., Simpson, C., 2003. High strain-rate deformation fabrics characterize a kilometers-thick Paleozoic fault zone in the Eastern Sierras Pampeanas, central Argentina. Journal of Structural Geology 25, 909–922.
Whitmeyer, S.J., Simpson, C., 2004. Regional deformation of the Sierra de San Luis, Argentina: implications for the Paleozoic development of western Gondwana. Tectonics 23, doi:10.1029/2003TC001542 TC1005.
Williams, M.L., Melis, E.A., Kopf, C.F., Hanmer, S., 2000. Microstructural tectonometamorphic processes and the development of gneissic layering: a mechanism for metamorphic segregation. Journal of Metamorphic Geology 18, 41–57.
Willner, A.P., 1990. División tectonometamórfica del basamento del noroeste Argentino. In: Aceñolaza, F.G., Miller, H., Toselli, A.J. (Eds.), El Ciclo Pampeano en el Noroeste Argentino, 4. Universidad Nacional de Tucumán, San Miguel de Tucumán, pp. 113–159.
Willner, A.P., Miller, H., 1982. Poliphase metamorphism in the Sierra de Ancasti (Pampean Ranges, NW Argentina) and its relation to deformation. In: Congreso Latinoamericano de Geología, 3, Buenos Aires, pp. 441-455.

Willner, A.P., Miller, H., 1985. Structural division and evolution of the Lower Paleozoic basement in the NW Argentine Andes. Zentralblatt für Geologie und Paleontologie I, 1245–1255.

Worley, B.A., Powell, R., Wilson, C.J.L., 1997. Crenulation cleavage formation: evolving diffusion, deformation and equilibration mechanism with increasing metamorphic grade. Journal of Structural Geology 19, 1121–1135.

Wu, S., Groshong, R.H., 1991. Low temperature deformation of sandstone, southern Appalachian fold-thrust belt. Bulletin of the Geological Society of America 103, 861–875.

Yang, X., Gray, D.R., 1994. Strain, cleavage, and microstructure variations in sandstone: implications for stiff layer behaviour in chevron folding. Journal of Structural Geology 16, 1353–1365.